Rare Met. (2023) 42(6):1778–1799
https://doi.org/10.1007/s12598-022-02234-4

RARE METALS

MINI REVIEW

Design strategies of Pd-based electrocatalysts for efficient oxygen reduction

Chun-Jie Li, Guang-Cun Shan, Chun-Xian Guo*, Ru-Guang Ma*

Received: 25 August 2022 / Revised: 20 September 2022 / Accepted: 22 September 2022 / Published online: 30 March 2023

Abstract Oxygen reduction reaction (ORR) occurs at the cathode of fuel cells and metal–air batteries, but usually suffers from sluggish kinetics. To solve this issue, efficient electrocatalysts are highly desired. Palladium (Pd)-based nanomaterials, as the most promising substitute of platinum (Pt), exhibit superior activity and stability in ORR electrocatalysis. The delicate regulation of the structure and/or composition shows great potential in improving the electrocatalytic ORR performance of Pd-based nanomaterials. In this review, we retrospect the recent advance of Pd-based ORR electrocatalysts, and analyses the relationship between nanostructure and catalytic performance. We start with the ORR mechanism and indicators of ORR performance in both alkaline and acidic media, followed by the synthetic methods for Pd-based nanoparticles. Then, we emphasize the design strategies of efficient Pd-based ORR catalysts from the perspective of composition, crystal phase, morphology, and support effects. Last but not least, we conclude with possible opportunities and outlook on Pd-based nanomaterials toward ORR.

Keywords Oxygen reduction reaction (ORR); Palladium (Pd); Electrocatalyst; Overpotential; Reaction kinetics

C.-J. Li, C.-X. Guo*, R.-G. Ma*
School of Materials Science and Engineering, Suzhou University of Science and Technology, Suzhou 215009, China
e-mail: cxguo@usts.edu.cn

R.-G. Ma
e-mail: ruguangma@usts.edu.cn; maruguang@mail.sic.ac.cn

G.-C. Shan
School of Instrumentation Science and Opto-electronics Engineering, Beihang University, Beijing 100083, China

1 Introduction

To alleviate global warming and environmental pollution, carbon neutrality becomes a significant topic and leads to a critical need for the alternatives of fossil fuels [1, 2]. Various of clean energy and devices, such as hydrogen, fuel cells (FCs) and metal–air batteries (MABs) have attracted extensive interests of worldwide researchers, due to high energy-conversion efficiency and environmental friendliness [3–6]. The cathodic reaction for both FCs and MABs is the oxygen reduction reaction (ORR), which is a critical rate-determining reaction owing to the sluggish kinetics [7–9]. Therefore, the development of high-efficiency ORR electrocatalysts is of great significance for their widespread applications.

At present, Pt-based materials are still the benchmark electrocatalyst for their superior ORR activity [10, 11]. However, there are some disadvantages for Pt-based ORR electrocatalysts, such as the scarcity of noble metal Pt, the poor methanol resistance and inferior durability [12, 13]. In the past decades, a great amount of non-Pt materials have been studied as promising ORR electrocatalysts, such as non-Pt noble metals [14, 15], transition metal-based nanomaterials [16, 17], and carbon-based materials [18, 19]. Among them, Pd-based nanomaterials have been regarded as a kind of prospective alternatives to Pt, due to the unique properties. On the one hand, Pd possesses similar crystal structure with Pt and exhibits excellent electrocatalytic activity in ORR [20, 21]. On the other hand, Pd is more abundant in the crust of Earth and more cost-effective relative to Pt [22]. In addition, Pd-based materials are more tolerant of methanol, thus leading them to be promising ORR electrocatalysts [23]. In recent years, many researchers have paid attention to developing

efficient Pd-based ORR electrocatalysts and the relevant publications have gradually increased as shown in Fig. 1.

In general, electrocatalytic performance of nanomaterials, including activity and stability, is highly related to their composition, morphology, crystal phase, and support materials [24]. Pd-based alloys usually show advantages relative to monometallic Pd in electrocatalysis. The doping or substitution of other metal or nonmetal elements could change the electronic structure of Pd and results in the strain of Pd lattice, which makes great contribution to the improved electrocatalytic ORR activity and/or stability [25, 26]. The architecture of nanoparticles has an important impact on their electrocatalytic properties. Compared with the nanoparticles with smooth surface, Pd-based nanomaterials with rough surface possess larger surface areas, thus exhibiting remarkably enhanced electrocatalytic performance. For instance, porous Pd nanosheets [27], nanoporous PdCr alloys [28], PdCuAu nanothorn assemblies [29] have been reported to exhibit superior electrocatalytic ORR performance.

To gain insights into the development of advanced Pd-based ORR electrocatalysts, the latest achievements on Pd-based nanomaterials were summarized and the underlying structure-performance relationship was analyzed in this review. We start with the electrocatalytic mechanism of ORR and indicators of electrocatalytic performance, then present the synthetic methods of Pd-based nanomaterials applied in ORR electrocatalysis. We focus on the design strategies to improve the electrocatalytic performance and several critically influential factors were pointed out, such as composition, morphology, crystal phase, and support materials. At last, the outlook on the potential opportunities and challenges for the future development of Pd-based ORR electrocatalysts were provided.

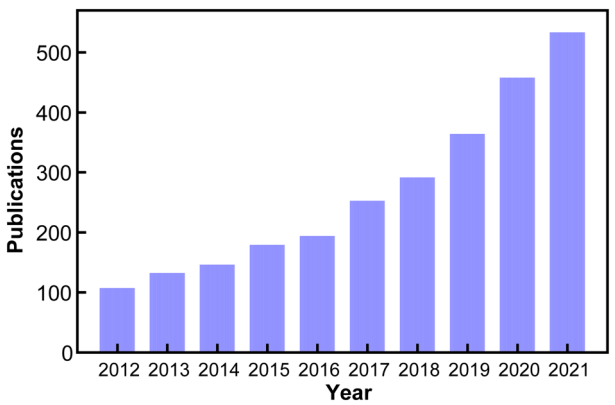

Fig. 1 Number of published papers in recent ten years containing "Pd" and "ORR" as topics (source: Web of Science database; date of search: 19 September 2022)

2 Electrocatalytic mechanism

2.1 Reaction pathway

In general, ORR occurs through two possible pathways. One pathway is the direct four-electron reaction, which is desirable in FCs and MABs. By this pathway, O_2 is directly reduced to H_2O or hydroxyl groups, without the production of hydrogen dioxide. The other one is the two-electron reduction reaction, by which hydrogen dioxide is generated as the intermediate and then further reduced to water [7, 11]. To be specific, the overall reaction in acidic condition is [30]:

$$O_2 + 4H^+ + 4e^- \rightarrow 2H_2O \quad (4e\ \text{pathway}) \tag{1}$$

$$O_2 + 2H^+ + 2e^- \rightarrow H_2O_2 \quad (\text{Step 1, 2e pathway}) \tag{2}$$

$$H_2O_2 + 2H^+ + 2e^- \rightarrow 2H_2O \quad (\text{Step 2, 2e pathway}) \tag{3}$$

and in alkaline condition the overall reaction is [31]:

$$O_2 + 2H_2O + 4e^- \rightarrow 4OH^- \quad (4e\ \text{pathway}) \tag{4}$$

$$O_2 + H_2O + 2e^- \rightarrow HO_2^- + OH^- \quad (\text{Step 1, 2e pathway}) \tag{5}$$

$$HO_2^- + H_2O + 2e^- \rightarrow 3OH^- \quad (\text{Step 2, 2e pathway}) \tag{6}$$

When Pd-based nanoparticles are used as electrocatalysts, the direct four-electron reaction is dominated, although it has been reported that ORR occurs partly through two-electron reduction due to the existence of palladium oxides on the surface [32]. In addition, Pd shows higher ORR performance in alkaline conditions than that in acidic electrolytes, which could be attributed to the less anion adsorption in alkaline conditions [23, 33]. In previous reports, the electrocatalytic activity of Pd-based materials toward ORR in alkaline medium can match or surpass that of commercial Pt/C [20, 34].

2.2 Adsorption configuration

According to the oxygen dissociation barrier on the catalyst surface, the direct four-electron pathway can be proceeded by a dissociative or associative pathway (Fig. 2a) [35]. In acidic medium, the dissociative pathway takes place by the following steps [36]:

$$O_2 + 2* \rightarrow 2O^* \tag{7}$$

$$2O^* + 2H^+ + 2e^- \rightarrow 2HO^* \tag{8}$$

$$2HO^* + 2H^+ + 2e^- \rightarrow 2H_2O + 2* \tag{9}$$

Herein, * represents a site on the surface of catalysts.

While the associative pathway goes through the elementary steps:

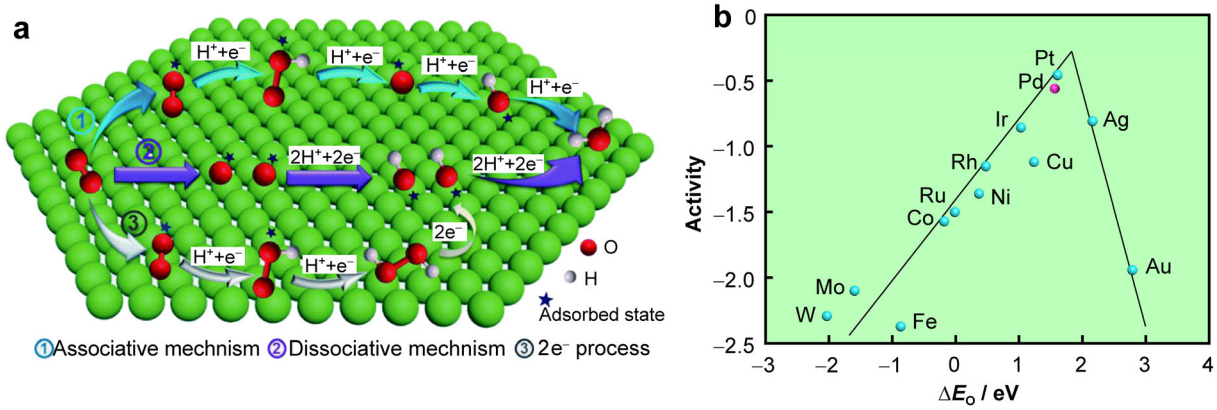

Fig. 2 **a** Scheme of different ORR mechanisms and resultant intermediates on surface of electrocatalysts. Reproduced with permission from Ref. [35]. Copyright 2019, the Royal Society of Chemistry. **b** A volcano map of ORR activity as a function of oxygen binding energy. Redrawn with permission from Ref. [36]. Copyright 2004, American Chemical Society

$$O_2 + * \rightarrow O_2^* \quad (10)$$

$$O_2^* + H^+ + e^- \rightarrow HOO^* \quad (11)$$

$$HOO^* + H^+ + e^- \rightarrow O^* + H_2O \quad (12)$$

$$O^* + H^+ + e^- \rightarrow HO^* \quad (13)$$

$$HO^* + H^+ + e^- \rightarrow H_2O + * \quad (14)$$

In alkaline condition, H_2O serves as the proton donor, and the corresponding steps in the ORR proceed as follows [37]:

$$\text{Dissociative pathway}: \ O_2 + 2^* \rightarrow 2O^* \quad (15)$$

$$2O^* + 2H_2O + 2e^- \rightarrow 2HO^* + 2OH^- \quad (16)$$

$$2HO^* + 2e^- \rightarrow 2OH^- + 2^* \quad (17)$$

$$\text{Associative pathway}: \ O_2 + * \rightarrow O_2^* \quad (18)$$

$$O_2^* + H_2O + e^- \rightarrow HOO^* + OH^- \quad (19)$$

$$HOO^* + e^- \rightarrow O^* + OH^- \quad (20)$$

$$O^* + H_2O + e^- \rightarrow HO^* + OH^- \quad (21)$$

$$HO^* + e^- \rightarrow OH^- + * \quad (22)$$

The binding energies of the intermediates on various metal surfaces have been calculated, and the activities of different metals can be plotted as a function of the O binding energy (ΔE_O). A typical volcano profile can be obtained by correlating the relationship between electrocatalytic activity and ΔE_O, as shown in Fig. 2b. From the plot, it is seen that Pt and Pd locate at the top region with medium ΔE_O, suggesting they are the excellent electrocatalysts toward ORR [36]. Therefore, Pd-based nanomaterials are of great potential when applied in ORR electrocatalysis.

2.3 Indicators of ORR performance

In ORR electrocatalytic measurements, rotating disc electrode (RDE) system is usually adopted in a three-electrode cell. The working electrode rotates to promote the convection of electrolyte and alleviates the mass transfer effect during ORR tests. Cyclic voltammetry (CV) curves are recorded with N_2/Ar saturated in the electrolyte to estimate the background current. The ORR polarization curves are obtained in O_2 saturated electrolyte by linear sweep voltammetry (LSV) scanning with a RDE rotation rate of 1600 r·min^{-1} typically. The kinetic current of the electrocatalysts can be evaluated according to the Koutecky–Levich equation [24, 38]:

$$\frac{1}{j} = \frac{1}{j_k} + \frac{1}{j_{lc}} \quad (23)$$

$$j_{lc} = 0.62\, nFAD^{2/3}\gamma^{-1/6}\omega^{1/2}C_{O_2} \quad (24)$$

where j, j_k and j_{lc} are the actually measured, the kinetic and the diffusion-limited current densities, respectively, F is the Faraday constant, A is the geometric area of the electrode, D is the diffusion coefficient of O_2, γ is the kinetic viscosity of the solution, ω is the rotation speed of electrode (rad·s^{-1}), and C_{O_2} is the concentration of dissolved O_2 in the solution. The j_k is generally derived from the Koutecky–Levich plot (j^{-1} vs. $\omega^{1/2}$) at various rotation speeds.

The Tafel slope can be used to evaluate the elementary steps and the rate determining steps in ORR, and thus determine the reaction mechanism and kinetics. According to the Tafel equation: $\Delta\eta = a\Delta\lg j$, the Tafel slope a could be obtained by the division of a potential range ($\Delta\eta$) into a logarithmic current range ($\Delta\lg j$) [39]. The turnover

frequency (TOF) is related to the total number of molecules transformed into the desired product by a single active site per unit time. The TOF reveals the catalytic performance of a single site and the intrinsic kinetic activity of the catalysts. The higher TOF value corresponds to the more active site [40, 41].

To assess the ORR performance of the catalysts, specific activity and mass activity are often calculated. Specific activity is the kinetic current normalized by the active surface area, and mass activity can be obtained by the kinetic current generated per unit mass of noble metals. The electrochemically active surface area (ECSA) is important to evaluate the specific activity and mass activity of the electrocatalysts. In general, the ECSA can be estimated by CO-stripping method, which involves the oxidation of pre-adsorbed CO monolayers, or by hydrogen underpotential deposition (H_{upd}) method, which is obtained by integrating the H_{upd} regions from CV curves [42]. Different from Pt, Pd will adsorb a certain amount of hydrogen and make it impossible to quantitatively differentiate between H_{upd} and absorbed hydrogen (H_{abs}), so it is difficult to estimate the ECSA of Pd by H_{upd} method. It has been reported that the ECSA of Pd-based electrocatalysts can be determined by the Pd oxide reduction analysis, and the Coulombic charge determined by integrating current peak of PdO reduction is employed [43].

Stability is another important indicator for the practical application of ORR electrocatalysts. There are usually two methods to evaluate the stability. One is to measure the current–time (i–t) chronoamperometric response at a potential in the limiting-diffusion range at a rotation rate of 1600 r·min^{-1} in O_2-saturated solution. The current remains no obvious change with the increase of time, indicating a good stability. The other method is the accelerated stress test (AST) recommended by the U.S. Department of Energy (DOE), which is conducted by CV cycling between 0.6 and 1.0 V (vs. RHE) in O_2-saturated solution. The smaller the half-wave potential ($E_{1/2}$) changes compared to that of the initial cycle, the better the stability.

3 Synthesis of Pd-based nanoparticles

There are various synthetic methods for the preparation of Pd-based nanoparticles, such as chemical reduction method, electrochemical deposition method, dealloying method. Generally, the structure of nanomaterials will be affected by the synthetic strategy. Therefore, the proper use of synthetic method could modify the structure of Pd-based nanomaterials, thus further influences their electrocatalytic performance.

3.1 Chemical reduction method

Chemical reduction method is one of the most commonly used methods for the preparation of Pd-based nanoparticles. This method is often direct and simple. During the synthesis process, metal salts are usually used as precursors and reduced by reducing agents, including sodium borohydride [44], ascorbic acid [45], formaldehyde [46, 47], carbon monoxide [48], dimethylamine borane [49], etc. In the reduction process, the property of reducing agent, the addition of structure directing agent, and the reaction condition will affect the reaction kinetics and then make impacts on the morphology and physiochemical nature of the nanomaterials. For example, Fu et al. fabricated Pd and bimetallic PdAg nanoparticles with three-dimensional network structure by using $NaBH_4$ at room temperature [44]. Zhu and coworkers [50] prepared core–shell PdPb@Pd aerogels by employing $NaHPO_2$ as the multifunctional reducing agent (Fig. 3a, b). In the reduction reaction, hypophosphite could promote the gelation, so $NaHPO_2$ is an important factor in the formation of multiply-twinned aerogel structure with an ordered intermetallic phase. Pd and Au@Pd porous nanoparticles with perpendicular pore channels and ultrathin branches were reported by Huang et al. [51] (Fig. 3c, d). In the synthesis, hexadecylpyridinium chloride (HDPC) was utilized as the structure-directing agent, while ascorbic acid served as the reducing agent. The use of HDPC contributes to the unique porous structure due to the special polarizability and compactness of the headgroup. When HDPC is absent or replaced with poly(vinyl pyrrolidone) (PVP) or hexadecyltrimethylammonium chloride (CTAC), the desired structure cannot be obtained. In addition, the reducing agent, ascorbic acid, is also critical in the reaction, its mild reducing ability benefits to the preparation of the unique well-defined porous structure. By using the same reducing agent with the assistance of poly(styrene)-b-poly(ethylene oxide) (PS-b-PEO) polymeric micelles, Li et al. [52] synthesized mesoporous Pd nanoparticles as shown in Fig. 3e, f. In this work, a series of comparison experiments were designed and the results showed that the porous structure and particle size would be affected by the reaction conditions, including the Pd precursor concentration, surfactant concentration, as well as the solvent composition.

3.2 Electrochemical deposition method

Electrochemical deposition (ED) provides an efficient strategy for the synthesis of Pd-based nanomaterials. By regulating the electrochemical parameters, the growth rate and structure of Pd-based nanomaterials can be rationally

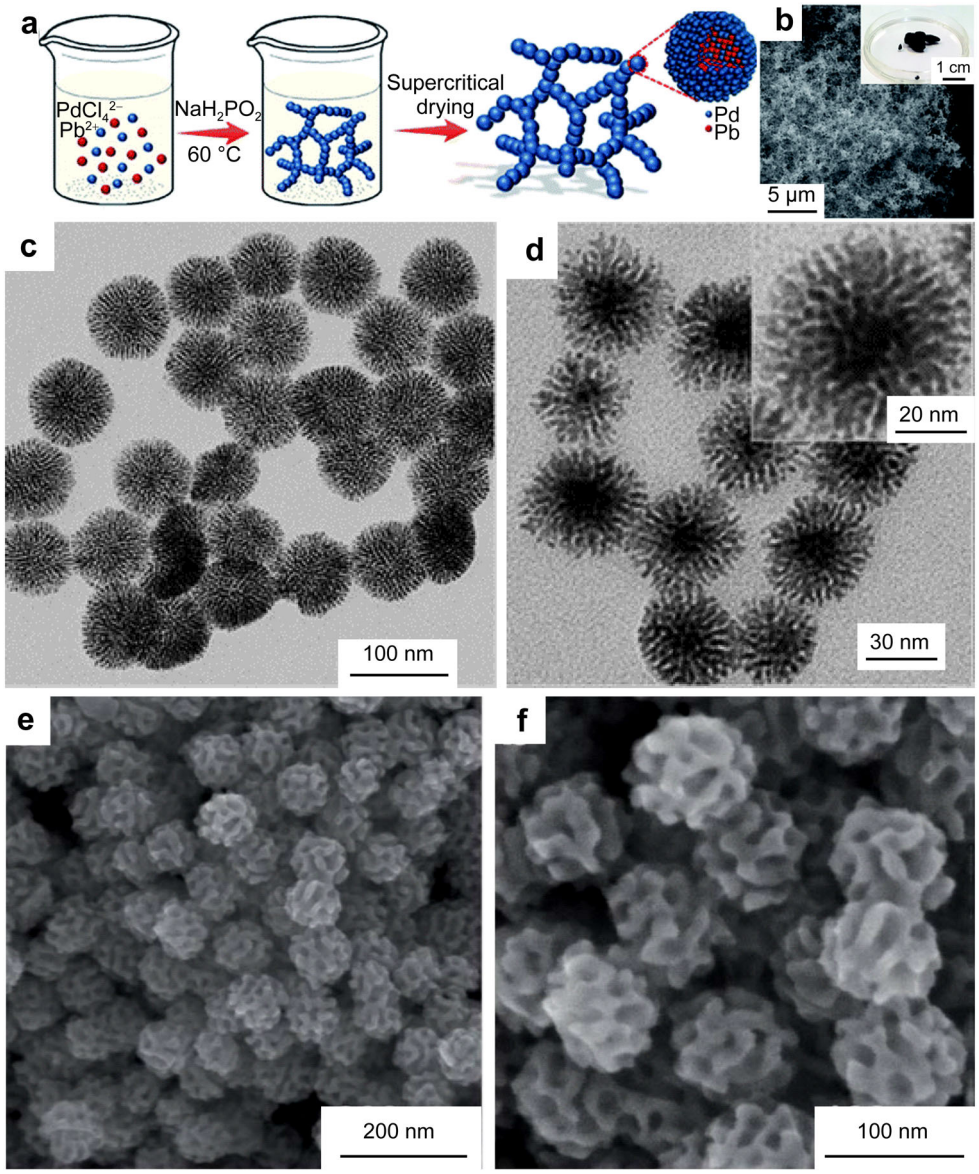

Fig. 3 **a** Illustration for synthesis of multiply-twinned PdPb@Pd aerogels; **b** SEM image of Pd_3Pb_1@Pd aerogel. Reproduced with permission from Ref. [50]. Copyright 2018, the Royal Society of Chemistry. TEM images for **c** porous palladium nanostructures and **d** porous Au@Pd nanostructures. Reproduced with permission from Ref. [51]. Copyright 2013, Wiley–VCH. **e**, **f** SEM images of mesoporous Pd nanoparticles. Reproduced with permission from Ref. [52]. Copyright 2019, the Royal Society of Chemistry

adjusted. In the process, two or three electrode configurations were used, and the electrolyte acts as both Pd precursor and conductive medium [53–55]. Recently, Pd-based materials with various morphologies have been prepared by ED method, such as nanowires [56], nanorods [57], nanourchins [58], nanoflake [59], nanoplates array [60]. For example, Xu et al. [61] fabricated highly ordered Pd nanowire arrays by employing anodized aluminum oxide (AAO) as the template. The obtained Pd nanowire arrays are composed of Pd nanowires with uniform diameter and length, and the nanowires are well isolated, parallel to each other, and perpendicular to the substrate. Zhao et al. [62] synthesized Pd dendritic nanostructures on single-crystal n-GaN(0001) by cyclic voltammetry. The deposition process was carried out at 0.2 V (vs. Ag/AgCl) without underpotential deposition process and followed the typical instantaneous nucleation in large overpotential region. The prepared nanoarchitecture contains numerous small branches around the trunk of dendritic structures and grows along the <111> directions, which is beneficial to the enhanced electrocatalytic performance. Su et al. [63] reported that 5 nm-thick Pd nanosheets could be obtained by electrochemical depositing Pd between graphene oxide (GO) sheets, due to the self-limiting growth. During the electrochemical deposition, a two-electrode

system containing a Pt anode and a GO-coated indium tin oxide (ITO) glass cathode was used, and $Pd(NO_3)_2$ aqueous solution served as the electrolyte. In this work, the thickness of the Pd nanosheets was not affected by growth time, because after full coverage of GO layers, the growth self-terminated.

Yamauchi et al. reported mesoporous Pd films with perpendicular mesochannels prepared by ED method [64]. In the synthesis, cationic surfactant, cetylmethylammonium chloride (C_{16}TAC), and Na_2PdCl_4 were mixed as the electrolyte, and Au substrate served as the working electrode. Under optimized conditions, the electrochemical deposition of Pd films was conducted at a constant potential. As shown in Fig. 4a–d, the as-prepared Pd films are featured with vertically aligned mesochannels. Distinct mesopores are uniformly distributed on the top surface (Fig. 4a, b). And the cross-sectional transmission electron microscopy (TEM) images suggest that cylindrical channels are distributed perpendicularly to the substrate (Fig. 4c, d). The unique structure could provide ultrahigh surface area, which is beneficial to the increased electrocatalytic performance. Similarly, in another work, they prepared mesoporous bimetallic PdCu films by the same method in nonionic micellar solutions (Fig. 4e) [65]. The as-synthesized PdCu films are filled into the mesochannels vertically aligning on the substrate as shown in Fig. 4f–i.

3.3 Dealloying method

Dealloying involves the selective dissolution of the active components from an alloy by chemical or electrochemical strategies, and the residual compounds (usually refers to noble metals) form unique structures after migration and diffusion [66, 67]. The dealloying method is easy to operate and the morphology and composition of the nanomaterials can be precisely controlled. Pd-based bimetallic and multi-metallic nanomaterials have been prepared by dealloying method, demonstrating advantages in the field of electrocatalysis. For example, Liu and Xu [68] synthesized nanoporous PdTi alloys by dealloying method. In the synthetic process, ternary PdTiAl was used as the precursor. After the simple dealloying at room temperature, nanoporous PdTi alloy was obtained, which had uniform ligament size and controllable bimetallic ratio. As shown in Fig. 5a, b, PdTi alloy possesses three-dimensional bicontinuous network nanostructure with interconnected pore channels, which are beneficial for the mass transport and largely contribute to the improved

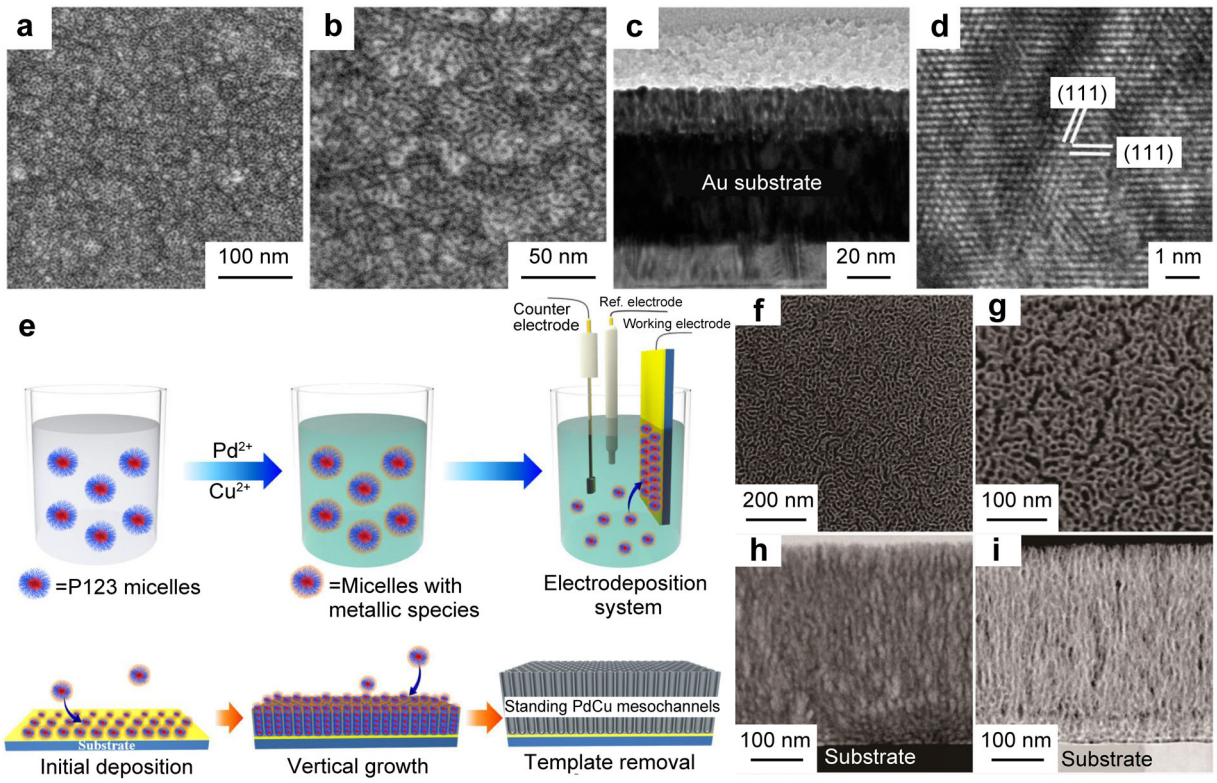

Fig. 4 **a**, **b** Top-view SEM images and **c**, **d** cross-sectional TEM images of mesoporous Pd films. Reproduced with permission from Ref. [64]. Copyright 2015, American Chemical Society. **e** Schematic illustration for formation of mesoporous PdCu films with vertical mesochannels; **f**, **g** Top-view SEM images, **h** TEM image and **i** HAADF-STEM cross-sectional image of mesoporous $Pd_{81}Cu_{19}$ films. Reproduced with permission from Ref. [65]. Copyright 2018, American Chemical Society

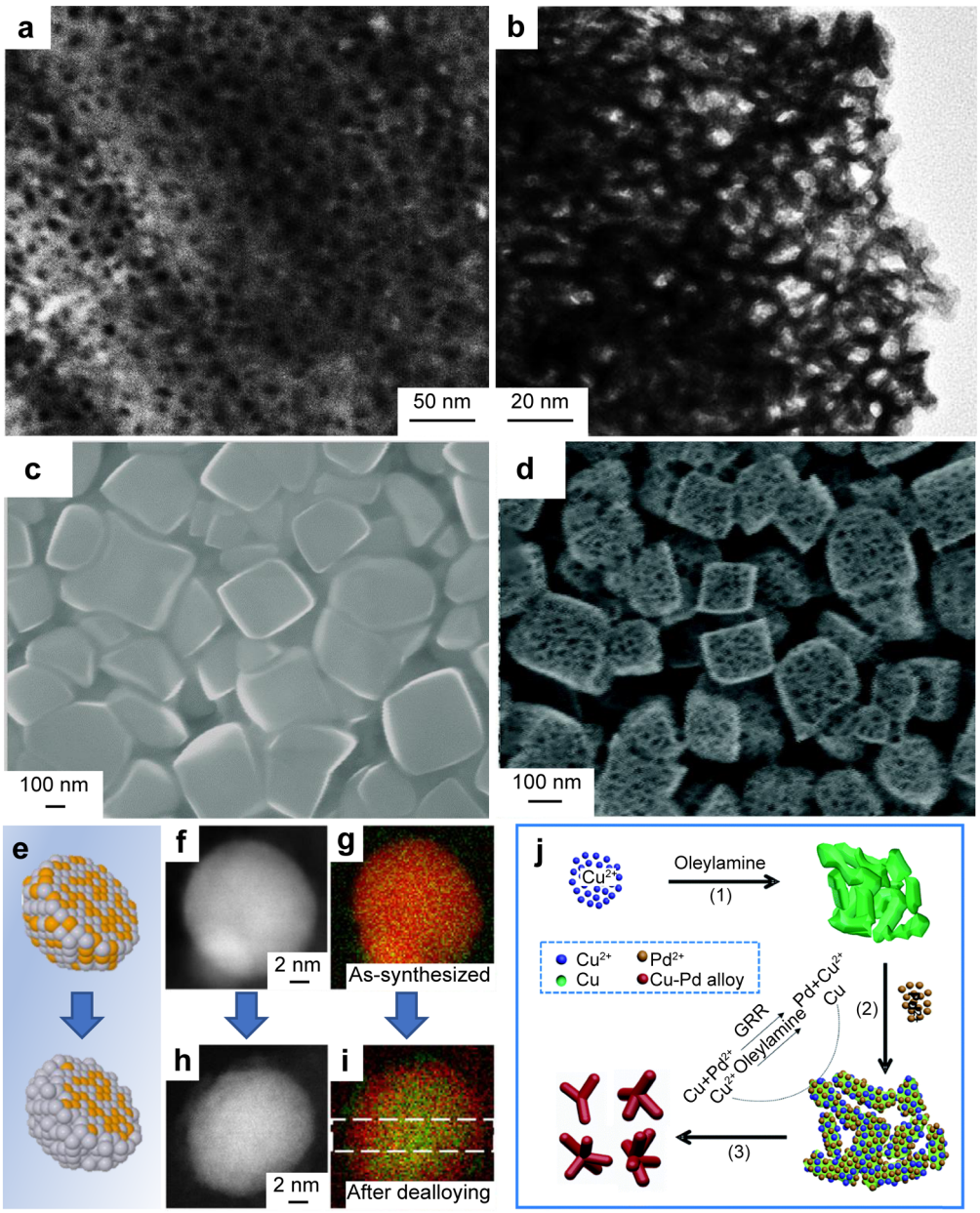

Fig. 5 **a** Top-view SEM and **b** TEM images of nanoporous PdTi alloy. Reproduced with permission from Ref. [68]. Copyright 2013, Wiley–VCH. **c**, **d** SEM images of **c** $Pd_{15}Ce_5Al_{80}$ alloy ribbon and **d** nanoporous PdCe nanocubes. Reproduced with permission from Ref. [69]. Copyright 2018, the Royal Society of Chemistry. **e** Illustration of electrochemical dealloying process of Pd/Ni or Pd/Mn; **f** STEM image and **g** corresponding elemental mapping images of Pd (red) and Ni (green) for PdNi/C before alloying; **h** STEM image and **i** corresponding elemental mapping images for PdNi/C after alloying. Reproduced with permission from Ref. [71]. Copyright 2020, American Chemical Society. **j** Illustration of synthesis of bimetallic CuPd alloy multipods by GRR from Ref. [79]. Copyright 2017, the Royal Society of Chemistry

electrocatalytic performance. Chen et al. [69] fabricated nanoporous PdCe nanocubes by a one-step chemical dealloying method from $Pd_{15}Ce_5Al_{80}$ alloy ribbons (Fig. 5c, d). The average size of the obtained nanoporous PdCe nanocubes is 200 nm, while the average pore size is about 5 nm. The highly conductive network and accessible open porosity could promote the electron and mass transportation in electrocatalysis. Sun et al. [70] reported the ordered intermetallic Pd_3Bi nanoparticles converted by colloidally synthesized ordered intermetallic $PdBi_2$ via electrochemical dealloying method. After the dissolution of Bi from the outer, the residual defect-rich amorphous material enables the transportation of Bi from the core, and results in reconstruction of the core to be a crystalline intermetallic. Furthermore, dealloying method could also be used as an effective way to enhance the

Table 1 ORR performances of Pd-based nanomaterials with different compositions

Catalysts	Electrolyte	Half-wave potential / V (vs. RHE)	Specific activity at 0.9 V (vs. RHE) / ($mA·cm^{-2}$)	Mass activity at 0.9 V (vs. RHE) / ($mA·mg^{-1}$)	Refs.
$Au@Pd_{0.17}$ structures	0.1 $mol·L^{-1}$ KOH	0.580	–	–	[81]
$Au@Pd_{0.5}$ structures		0.710			
$Au@Pd_{1.0}$ structures		0.850			
$Au@Pd_{1.5}$ structures		0.830			
nPd/C	0.1 $mol·L^{-1}$ NaOH	0.807	–	35.5	[82]
Ir_8Pd_{92}/C		0.838		46.8	
$Ir_{23}Pd_{77}$/C		0.840		55.8	
$Ir_{37}Pd_{63}$/C		0.835		39.8	
Mesoporous PdRu nanocrystals	0.1 $mol·L^{-1}$ KOH	0.910	2.90	1550	[83]
$Rh_{80}Pd_{20}$ cube	0.1 $mol·L^{-1}$ $HClO_4$	–	0.15	10	[84]
$Rh_{62}Pd_{38}$ cube			0.04	6	
$Rh_{43}Pd_{57}$ octahedron			0.03	11	
$Rh_{29}Pd_{71}$ octahedron			0.19	55	
Rh_8Pd_{92} octahedron			0.24	101	
Nanoporous Pd-Cu thin films	0.1 $mol·L^{-1}$ KOH	0.896	1.42	1110	[85]
Nanoporous PdCr alloys	0.1 $mol·L^{-1}$ $HClO_4$	–	0.24	160	[28]
PdAuBiTe nanosheets	0.1 $mol·L^{-1}$ KOH	0.929	3.93	2480	[88]
PdBiTe nanosheets		0.897	1.27	730	
Au-O-PdZn/C	0.1 $mol·L^{-1}$ KOH	–	–	105	[89]
D-PdZn/C				56	
O-PdZn/C				78	
Pd_3Pb ultrathin porous intermetallic nanosheets	0.1 $mol·L^{-1}$ KOH	0.908	1.18	590	[90]
Pd_4S/C	0.1 $mol·L^{-1}$ KOH	0.877	–	–	[91]
B-doped Pd particle	0.1 $mol·L^{-1}$ KOH	0.860	4.13 at 0.85 V	2380 at 0.85 V	[92]
BiPd/C_Pre	0.1 $mol·L^{-1}$ KOH	0.860	0.604	752	[93]
PbPd/C_Pre		0.840	0.466	641	
SnPd/C_300		0.810	0.525	292	
CuPd@NiPd nanoparticles	0.1 $mol·L^{-1}$ KOH	0.910	2.840	250	[94]
Alloy CuPd		0.880	–	170	
Alloy NiPd		0.870	–	190	

electrochemical performance of Pd-based nanoparticles. Lu et al. [71] discovered that Pd/Ni and Pd/Mn nanoparticles showed enhanced ORR activity after the electrochemical dealloying. This was because that Ni or Mn selectively leached out during the dealloying process, and electrochemically active Pd enriched at the surface of Pd/Ni and Pd/Mn nanoparticles (Fig. 5e–i). Not only does the core–shell structure contribute to the improved ORR ability, but also does the reduced surface oxide after electrochemical dealloying. In addition, other Pd-based nanoparticles with various features have also been prepared by dealloying method, such as hierarchical nanoporous Pd [72], core–shell Pd–M (M=Fe, Co and Ni) nanoparticles with Pd_3M core and Pd shell [73], nanoporous bimetallic Ag–Pd alloys [74], and nanoporous Pd/NiO composites [75].

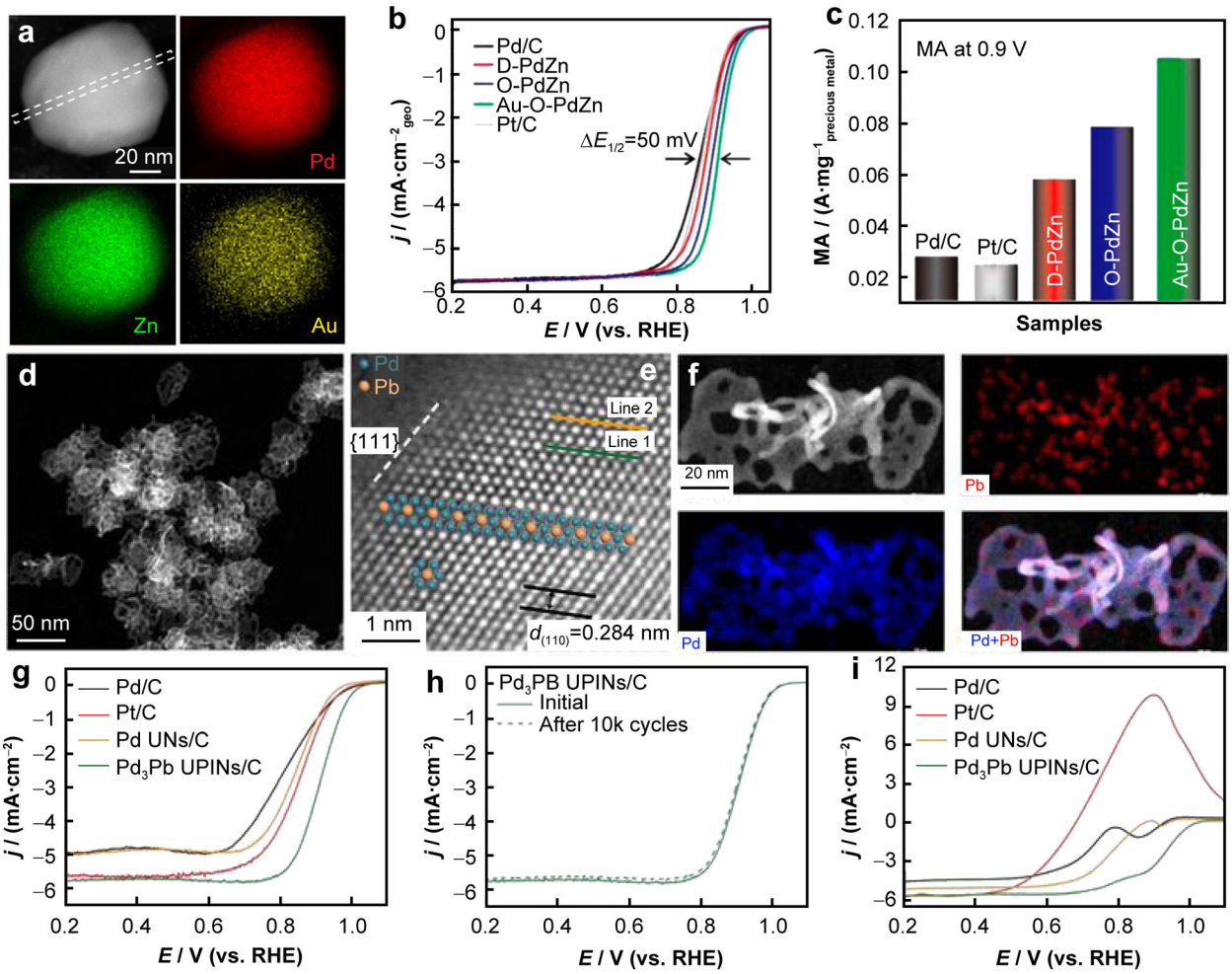

Fig. 6 **a** STEM and corresponding elemental mapping images of Pd, Zn and Au; **b** polarization profiles of different electrocatalysts toward ORR; **c** mass activity of different electrocatalysts at 0.9 V (vs. RHE). Reproduced with permission from Ref. [89]. Copyright 2019, American Chemical Society. **d** HAADF-STEM, **e** atomic-resolution aberration-corrected HAADF-STEM, and **f** STEM-EDX elemental mapping images of Pd_3Pb ultrathin porous intermetallic nanosheets (UPINs); **g** polarization curves for Pd_3Pb UPINs/C (green), Pd UNs/C (orange), Pt/C (red), and Pd/C (black) electrocatalysts toward ORR; **h** polarization curves of Pd_3Pb UPINs/C before and after cycling test; **i** polarization curves of different electrocatalysts with addition of methanol. Reproduced with permission from Ref. [90]. Copyright 2021, Wiley–VCH

3.4 Other methods

Apart from the above-mentioned synthetic methods, Pd-based nanomaterials can also be prepared by various strategies, such as hydrothermal method, galvanic replacement method, hard template method. Lim et al. [76] prepared Pd nanorods and nanowires by a hydrothermal method at 200 °C with $PdCl_2$ as the precursor. In the synthesis, the high yield of these one-dimensional (1D) nanostructures is tuned by the addition of low concentrations of Cu^{2+} and/or NaCl, in which Cu ions could scavenge oxygen to suppress etching of the twinned Pd seeds that grow into nanowires, and the addition of NaCl will lower the reduction rate due to the formation of $PdCl_4^{2-}$, thus promotes diffusional growth. When the molar ratio of Cu to Pd was ~ 1:12,500, the yield of 1D nanostructures could increase from 10% to 90%. Meanwhile, NaCl could enhance the growth of 1D structure, so long Pd nanowires could be obtained in high yield. Kong et al. [77] fabricated Pd porous hollow spheres by a template method. In the study, SiO_2 colloids were used as the template material, and Pd was electroless plated. After the removal of SiO_2 by NaOH aqueous solution, porous hollow Pd spheres were prepared. In addition, AAO was also used as template to synthesize Pd nanowire arrays by Li et al. [78]. The reduction reaction occurred in the pores of AAO, and Al sheet in the bottom of pores served as a reductant in reducing Pd^{2+} ions attracted into the pores under hydrothermal conditions. Chen et al. [79] prepared bimetallic CuPd alloy multipods by a galvanic replacement

strategy. In the synthesis, Cu nanoparticles were firstly fabricated as the sacrificed template, and after the addition of Pd precursor, the galvanic replacement reaction (GRR) would occur between Cu templates and Pd^{2+}, as illustrated as Fig. 5j. During the reaction, Pd^{2+} were reduced to metallic Pd, while Cu seeds were oxidized to Cu^{2+}. The resultant Cu^{2+} were simultaneously reduced by oleylamine, thus leading to the formation of CuPd alloy multipods. The obtained CuPd multipods possess an average diameter of about 15.5 nm. And there are various types of multipods, including tripods, tetrapods, pentapods and hexapods. The unique microstructure, electron transfer from Cu to Pd, and lattice contraction of Pd imposed by Cu collectively contribute to the enhanced electrocatalytic activity.

4 Design strategies

The electrocatalytic performance of catalysts will be affected by their intrinsic properties including composition, morphology, crystal phase, support materials, and so on. In ORR electrocatalysis, the optimization of these aspects may contribute to the enhanced electrocatalytic activities of Pd-based nanoparticles.

4.1 Composition regulation

Relative to mono-metallic Pd, Pd-based bimetallic and multi-metallic nanoparticles exhibit significant advantages in ORR electrocatalysis. The incorporation of suitable metal elements would regulate the electronic configuration of Pd and alter the strength of oxygen adsorption, thus enhance the electrocatalytic ORR activity [23, 80]. It has been reported that Pd has combined with a variety of metal elements to form promising ORR electrocatalysts, such as Au [81], Ir [82], Ru [83], Rh [84], Cu [85], Ni [86], Co [87], Cr [28] (Table 1). For example, Zhao et al. [88] proposed a visible-light-induced template strategy to synthesize two-dimensional ultrathin PdAuBiTe alloy nanosheets. The obtained nanosheets possess the thickness of $\sim$ 5 nm and the diameters of more than 500 nm, and the ratio of horizontal to vertical surpasses 100. Benefitting from the combination of topmost and edge defects, low-coordinated atoms, lattice strain, and downshift of the d-band center of Pd, the PdAuBiTe alloyed nanosheets exhibit enhanced ORR performance with longer durability and higher mass activity. Meanwhile, PdAuBiTe nanosheets also show higher methanol tolerance and poison tolerance to CO relative to commercial Pd/C and Pt/C. Yang and coworkers [89] synthesized an ordered intermetallic

Table 2 ORR performances of Pd-based nanomaterials with different morphologies

Catalysts	Electrolyte	Half-wave potential / V (vs. RHE)	Specific activity at 0.9 V (vs. RHE) / ($mA{\cdot}cm^{-2}$)	Mass activity at 0.9 V (vs. RHE) / ($mA{\cdot}mg^{-1}$)	Refs.
PdCuAu nanothorn assemblies	0.1 $mol{\cdot}L^{-1}$ $HClO_4$	0.860	–	–	[29]
Hyper-dendritic PdZn nanocrystals	0.1 $mol{\cdot}L^{-1}$ KOH	0.910	0.393	461	[97]
Intermetallic Pd_3Pb nanowire networks	0.1 $mol{\cdot}L^{-1}$ KOH	–	15.7	610	[98]
PdNi nanocorals	0.1 $mol{\cdot}L^{-1}$ KOH	0.851	–	6.03	[99]
CuPd alloy multipods	0.1 $mol{\cdot}L^{-1}$ $HClO_4$	0.818	–	–	[79]
CuPd alloy nanospheres		0.807			
Nanoporous PdCe nanocubes	0.1 $mol{\cdot}L^{-1}$ KOH	–	–	78.2	[69]
Pd metallene/C	0.1 $mol{\cdot}L^{-1}$ KOH	0.900	1.336	892	[101]
Pd_4Sn wavy nanowires	0.1 $mol{\cdot}L^{-1}$ KOH	0.929	1.51	650	[102]
Ordered Pd_2Sn nanosheets	0.1 $mol{\cdot}L^{-1}$ KOH	0.893	9	2500	[103]
PdCuMo porous nanosheets	0.1 $mol{\cdot}L^{-1}$ KOH	0.913	0.64	1460	[104]
Ultrathin AuPd nanowires	0.1 $mol{\cdot}L^{-1}$ KOH	0.900	1.98 at 0.85 V	770 at 0.85 V	[105]

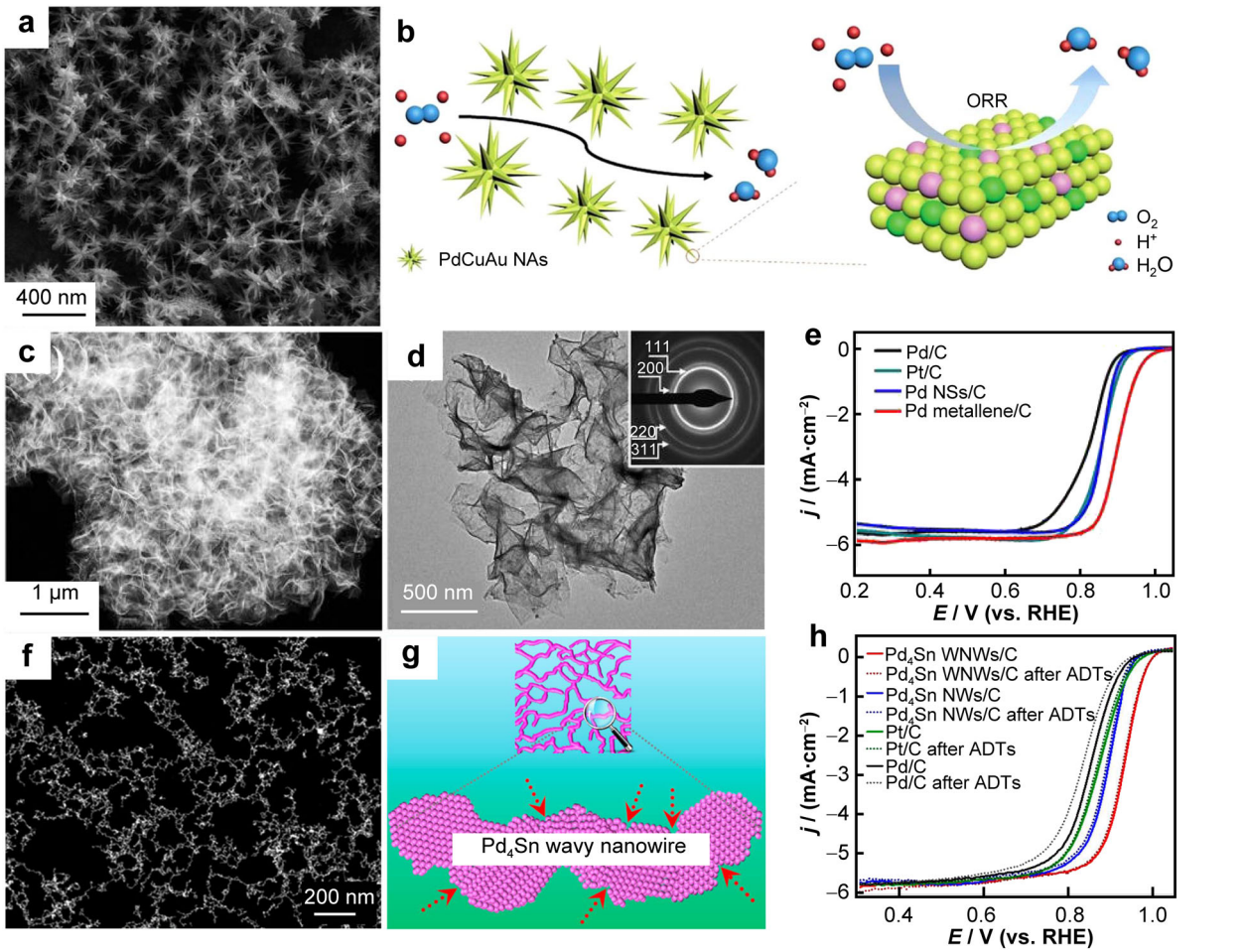

Fig. 7 **a** SEM image of PdCuAu nanothorn assemblies; **b** schematic illustration of ORR electrocatalysis on PdCuAu nanothorn assemblies. Reproduced with permission from Ref. [29]. Copyright 2018, the Royal Society of Chemistry. **c** HAADF-STEM and **d** TEM images of porous Pd metallene; **e** ORR polarization curves of different catalysts. Reproduced with permission from Ref. [101]. Copyright 2021, Wiley–VCH. **f** HAADF-STEM image and **g** schematic diagram of Pd_4Sn wavy nanowires; **h** ORR polarization curves for different electrocatalysts before and after 10,000 cycles of accelerated durability tests (ADTs). Reproduced with permission from Ref. [102]. Copyright 2019, American Chemical Society

PdZn/C (O-PdZn) coated by a Pd shell with several atomic layers, and then incorporated Au. As shown in Fig. 6a, Au, Pd and Zn elements are dispersed uniformly in elemental mapping images, indicating that Au is homogeneously distributed through the nanoparticle. The experimental results indicate that PdZn alloying and the decoration of Au can weaken the oxygen affinity and enhance the electrocatalytic activity toward. The polarization curves suggest that the half-wave potential ($E_{1/2}$) of O-PdZn, disordered PdZn (D-PdZn), and Au-incorporated O-PdZn (Au-O-PdZn) are higher by 20, 34 and 50 mV relative to those of Pd/C and Pt/C, respectively, as shown in Fig. 6b. Moreover, the mass activity of Au-O-PdZn/C at 0.9 V is obviously higher than those of D-PdZn/C, O-PdZn/C, Pt/C and Pd/C, demonstrating the significant composition advantage of Au-O-PdZn (Fig. 6c, Table 1). Other ultrathin porous Pd-M (M=Pb, Sn and Cd) intermetallic nanosheets were also reported by Guo and coworkers [90], which were synthesized by a template-directed method. When used as ORR electrocatalyst, Pd_3Pb porous nanosheets displayed enhanced activity, superior stability, and higher methanol tolerance relative to Pd ultrathin nanosheets, Pd/C and Pt/C (Fig. 6d–i). Theoretical calculations based on density functional theory (DFT) indicate that the interatomic interaction of Pd_3Pb intermetallic alloy could optimize the electronic structure, thus weakening the adsorption of OH intermediate and boosting the reaction kinetics.

Except for metal elements, researchers have recently found that the incorporation of non-metallic elements (e.g., S, B and P) can also help to enhance the ORR performance of Pd. For instance, Du et al. [91] prepared various palladium sulfides (e.g., $Pd_{16}S_7$, Pd_4S and PdS) by a one-pot colloidal method in hot solution. Among the sulfides, monodisperse Pd_4S nanoparticles displayed the best

electrocatalytic ORR performance in the alkaline. $E_{1/2}$ of Pd_4S nanoparticles was determined to be 0.877 V, with about 47 mV more positive relative to that of commercial Pt/C (Table 1). Meanwhile, the obtained Pd_4S nanoparticles also exhibited improved methanol tolerance and significantly enhanced stability compared with Pt/C catalyst. Theoretical calculations suggested that the existence of oxygen absorption sites at the surface of Pd_4S could anchor atomic O moderately and desorb O_2 molecule facilely, thus leading to improved ORR performance.

By combining DFT calculations with experiment results, Vo Doan et al. [92] explored the mechanism of enhanced ORR performance in B-doped Pd (Pd–B). On the basis of theoretical modelling, the intermediates absorb weakly on the surface of B-doped Pd relative to Pd during the ORR process. And Pd–B exhibits nearly optimal binding energy by lowering the energy barrier, which is associated with O_2 dissociation, indicating Pd–B would have high activity for ORR. Experimentally, B-doped Pd nanoparticles were prepared by an electroless deposition route and the ORR activity was evaluated. According to the results, B-doped Pd nanoparticles exhibit 2.5-fold and 8.8-fold higher specific activity and 14-fold and 35-fold higher mass activity than commercial Pd/C and Pt/C electrocatalysts, respectively. Based on the simulated Pd–B surface and XPS analysis, the binding energy of Pd–B nanoparticles is in lower value region compared with pure Pd, and most of the surface atoms of Pd–B catalyst possess higher electron density relative to Pd nanoparticles. The additional electrons could efficiently weaken the bonding strength between O and Pd atoms, thus decreasing the binding energy and enhancing the electrocatalytic ORR property of Pd–B. Rego et al. [95] reported a gas diffusion layer directly deposited by carbon-supported PdP nanocatalysts, where the P accounted for about 15 at%, and different Pd were loaded. The obtained PdP alloys exhibit higher activity compared with Pd toward ORR, but comparable to that of Pt in the acidic solution. And the results suggest that ORR occurring on PdP alloy proceeds through the 4e pathway.

4.2 Morphology modulation

Many studies indicate that morphology regulation plays a significant role in the improvement of electrocatalytic activity of ORR. The rational morphology control of catalysts could lead to the exposure of particular surfaces and influence catalytic active sites, thus affecting their catalytic properties [23, 96]. In recent years, Pd-based nanomaterials with controllable morphologies have been reported as excellent electrocatalysts with comparable performance to Pt/C catalyst toward ORR (Table 2). For instance, Wang et al. [29] fabricated PdCuAu nanothorn assemblies with a direct one-step method and the obtained materials were self-supported and assembled from staggered nanothorns. The highly branched architectures could provide sufficient accessible active sites in ORR electrocatalysis and the unique structure is not susceptible to particle agglomeration during the reaction (Fig. 7a, b). The combination of the branched morphology and tri-metallic composition renders PdCuAu nanothorn assemblies to be superior ORR catalyst with high electrocatalytic activity, durability, and methanol tolerance. Huang and coworkers [97] prepared three-dimensional (3D) hyper-dendritic PdZn nanocrystals by a one-pot pathway without templates and regulated by gas mixtures of CO and H_2. Benefitting from the porous nature, hyper-dendritic nanostructure and electronic modulation of Zn, the obtained catalysts exhibit superior ORR performance. The mass activity and specific activity of hyper-dendritic PdZn nanocrystals are determined to be 0.461 $A{\cdot}mg_{Pd}^{-1}$ and 0.393 $mA{\cdot}cm^{-2}$ at 0.9 V, which are 5.2-fold and 5.0-fold that of Pt/C, respectively. Besides, the catalyst also displayed improved stability with only 3% loss of mass activity after 10,000 cycles for ORR. Shi et al. [98] prepared intermetallic Pd_3Pb nanowire networks via a one-step wet-chemistry strategy. The obtained catalyst exhibited distinctly enhanced ORR activity and stability comparable to Pt/C electrocatalyst as well as improved methanol-tolerant ability. The superior electrocatalytic property is mainly ascribed to the unique microstructure

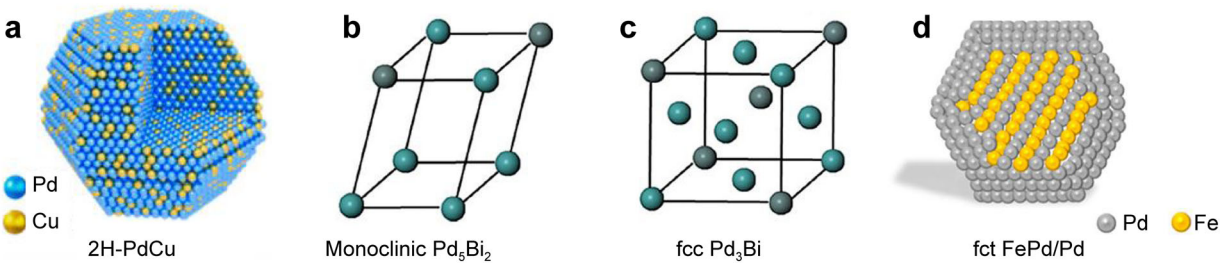

Fig. 8 Different crystal structure of Pd-based nanoparticles: **a** hcp 2H type PdCu alloy nanoparticles. Reproduced with permission from Ref. [108]. Copyright 2021, American Chemical Society. **b**, **c** Monoclinic Pd_5Bi_2 and fcc Pd_3Bi nanocrystals. Reproduced with permission from Ref. [109]. Copyright 2021, American Chemical Society. **d** fct-FePd/Pd nanoparticles. Reproduced with permission from Ref. [110]. Copyright 2015, American Chemical Society

Table 3 ORR performances of Pd-based nanomaterials with different crystal phases

Catalysts	Electrolyte	Half-wave potential / V (vs. RHE)	Mass activity at 0.9 V (vs. RHE) / ($mA \cdot mg^{-1}_{Pd}$)	Refs.
2H-$Pd_{67}Cu_{33}$ nanoparticles	0.1 $mol \cdot L^{-1}$ KOH	0.905	870	[108]
fcc $Pd_{69}Cu_{31}$ nanoparticles		0.883	350	
Monoclinic Pd_5Bi_2/C	0.1 $mol \cdot L^{-1}$ KOH	0.930	2050	[109]
fcc Pd_3Bi/C		0.924	920	
fcc-FePd	0.1 $mol \cdot L^{-1}$ $HClO_4$	0.840	34.8	[110]
fct-FePd		0.860	41.3	
fct-FePd/Pd		0.880	99.7	

and the formation of Pd_3Pb intermetallic phase. The ultrathin nanowires possess 3D porous structures with rough surfaces, which could provide a large number of opening channels for the outside and inside active sites to be accessible to catalyzing the fuel molecule. In addition, many other Pd-based efficient ORR catalysts with different morphologies have also been reported, such as 3D PdNi nanocorals [99], nanoporous PdCu films [85], Pd nanocubes [100], CuPd alloy multipods [79], nanoporous PdCe nanocubes [69].

Besides, the construction of defects in nanoparticles could modulate surface electronic structure and influence the electrocatalytic capacities. For example, Yu et al. [101] fabricated ultrathin porous Pd metallene with abundant lattice defects by a wet-chemistry method as an effective electrocatalyst toward ORR in alkaline medium. As shown in Fig. 7c, d, the prepared Pd metallene exhibits an ultrathin two-dimensional (2D) curved nanosheet architecture and the lateral dimension could reach to 500 nm. The curved ultrathin 2D structure, high porosity and abundant defects render Pd metallene to be promising electrocatalyst for ORR. As shown in Fig. 7e, the defect-rich porous Pd metallene/C displays better ORR activity than spherical Pd nanosheets/C, commercial Pt/C and Pd/C catalyst. The enhanced electrocatalytic activity mainly arises from the morphology of curved sub-nanometer nanosheet, which could endow the nanosheet with strain effect and regulate the electronic structure to adjust the binding strength of oxygen on Pd, thus facilitating the ORR property. Zhang et al. [102] synthesized 1D PdSn nanowires (NWs) with controllable defects consisting of Pd_4Sn wavy NWs with rich defects and Pd_4Sn NWs with penta-twinned nanostructures (Fig. 7f, g). The electrochemical results suggest that the PdSn NWs display defect-dependent properties, and the Pd_4Sn wavy NWs with rich defects present superior electrocatalytic activity and durability, as displayed in Fig. 7h. DFT calculations reveal that the surface defect region displays optimized electronic structure for charge transfer and structural flexibility, which effectively weaken the overbinding effect and boost the ORR activity. Liang et al. [103] fabricated ultrathin and intermetallic Pd_2Sn nanosheets with rich defects through a seed-mediated strategy. The obtained ordered Pd_2Sn nanosheets displayed superior ORR property and durability in alkaline condition relative to the disordered counterparts, Pt/C, and many reported Pd-based electrocatalysts for ORR. The remarkable ORR performance attributed to the advantageous 2D architecture with rich defects, the thermodynamically stable intermetallic structure, and the optimized Pd–O binding strength is due to Sn incorporation.

4.3 Crystal phase engineering

Except for composition and morphology, the crystal phase of Pd-based nanoparticles also plays a critical role in ORR electrocatalysis. The different electronic structures deriving from the diverse crystal lattices affect the intrinsic properties of nanomaterials, thus leading to different electrocatalytic capacities [106, 107]. Relative to the thermodynamically stable face-centered cubic (fcc) phase, Pd-based nanomaterials with unique crystal phases possess different characteristics, which could help to boost their electrocatalytic activity and stability. For example, Ge et al. [108] synthesized PdCu alloy nanoparticles with unconventional hexagonal close-packed (hcp, 2H type) phase with tunable Cu contents by a general seeded strategy (Fig. 8a). Furthermore, galvanic replacement reaction of Cu by Pt could lead to the formation of unconventional trimetallic 2H-PdCuPt nanoparticles. As seen in Table 3, the prepared unconventional 2H-$Pd_{67}Cu_{33}$ nanoparticles display improved ORR activity in alkaline condition, with a higher mass activity of 0.87 $A \cdot mg_{Pd}^{-1}$ at 0.9 V, which is 2.5-fold and 4.0-fold that of the conventional fcc $Pd_{69}Cu_{31}$ counterpart and Pd/C catalyst, respectively. The results reveal the importance of crystal phase on adjusting the ORR property. In addition, the ORR performance of the

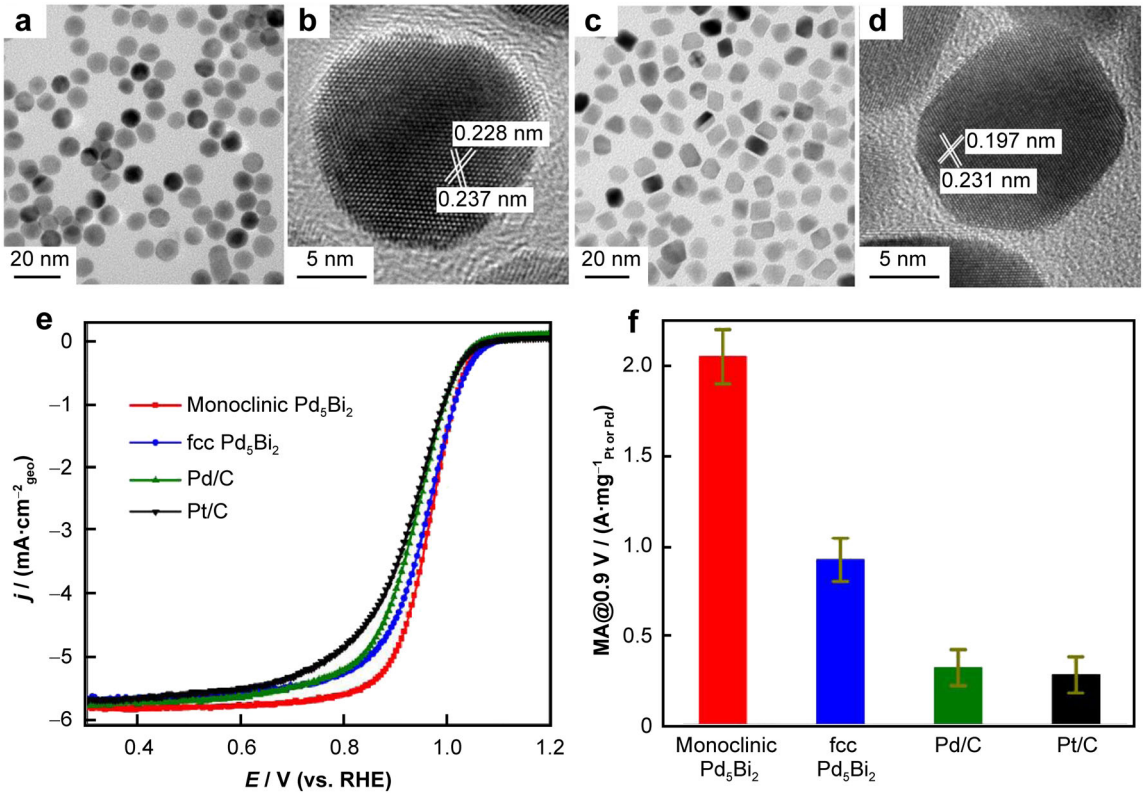

Fig. 9 **a** TEM and **b** HRTEM images of monoclinic Pd_5Bi_2 nanocrystals; **c** TEM and **d** HRTEM images of fcc Pd_3Bi nanocrystals. **e** ORR polarization curves of different catalysts; **f** mass activities of different catalysts at 0.9 V (vs. RHE). Reproduced with permission from Ref. [109]. Copyright 2021, American Chemical Society

Table 4 ORR performances of Pd-based nanomaterials with various support materials

Catalysts	Electrolyte	Half-wave potential / V (vs. RHE)	Specific activity at 0.9 V (vs. RHE) / ($mA·cm^{-2}$)	Mass activity at 0.9 V (vs. RHE) / ($mA·mg^{-1}$)	Refs.
Pd/SnO_2 catalyst	0.1 $mol·L^{-1}$ KOH	0.832	0.007	38	[118]
Thiolated GO-supported PdCo catalyst	0.1 $mol·L^{-1}$ KOH	0.810	2.08 at 0.8 V	329.13 at 0.8 V	[116]
GO-supported PdCo catalyst		0.750	0.99 at 0.8 V	115.55 at 0.8 V	
N-doped carbon nanotubes supported PdCoNi nanoparticles	0.1 $mol·L^{-1}$ KOH	0.907	3.78	252	[117]
Mo_2C-coupled Pd atomic layers	0.1 $mol·L^{-1}$ KOH	0.935	3.19	2055	[119]
$PdH_{0.706}$@Ni-B/C	0.1 $mol·L^{-1}$ $HClO_4$	0.910	–	1050	[120]
$PdH_{0.706}$/C		0.890		750	
Nano-hollow spherical PdCuMoNiCo NHSs/RGO_3-CNT	0.1 $mol·L^{-1}$ $HClO_4$	0.860	–	882 at 0.8 V 265 at 0.85 V	[5]
Pd/N-MoO_2-Mo_2C half-hollow nanotube	0.1 $mol·L^{-1}$ KOH	0.900	–	2360 at 0.8 V	[121]

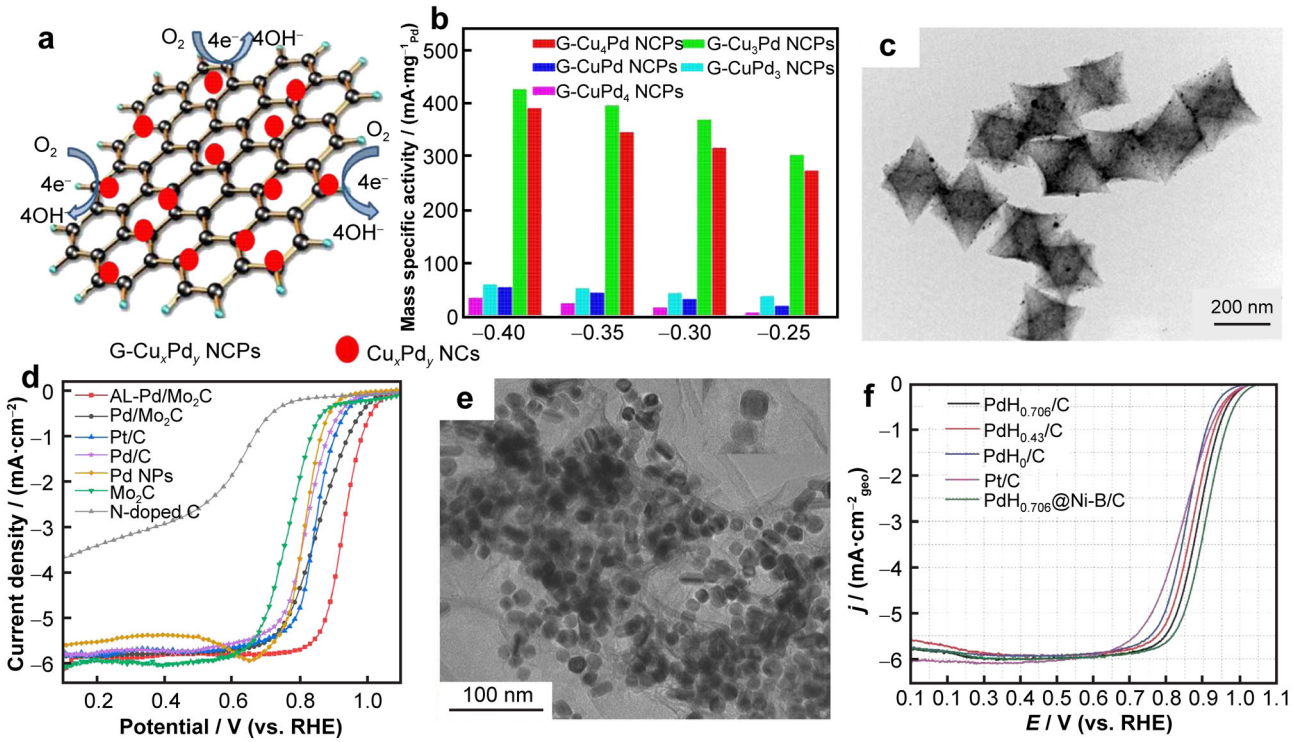

Fig. 10 **a** Schematic illustration of ORR electrocatalysis on G-Cu_xPd_y nanocomposites; **b** mass activities of G-Cu_xPd_y nanocomposites under different potentials. Reproduced with permission from Ref. [115]. Copyright 2015, American Chemical Society. **c** TEM image of AL-Pd/Mo_2C embedded in octahedral carbon frameworks. **d** ORR polarization curves of different catalysts. Reproduced with permission from Ref. [119]. Copyright 2021, American Chemical Society. **e** TEM image of $PdH_{0.706}$@Ni–B composites; **f** polarization curves of PdH_x with different *x* value, Pt/C and $PdH_{0.706}$@Ni–B/C catalysts. Reproduced with permission from Ref. [120]. Copyright 2017, Wiley–VCH

nanoparticles with the incorporation of Pt could be further enhanced. Zhou et al. [109] prepared monoclinic Pd_5Bi_2 and conventional fcc Pd_3Bi nanocrystals (Fig. 8b, c) and evaluated their ORR performance. The bimetallic nanocrystals with different crystal phase were fabricated under the same synthetic condition with different Pd precursors, and possessed comparable size and morphology (Fig. 9a–d). When applied in ORR electrocatalysis, the carbon-supported monoclinic Pd_5Bi_2 nanocrystals exhibit superior activity with a mass activity of 2.05 $A{\cdot}mg_{Pd}^{-1}$, which is higher than fcc structured Pd_3Bi nanocrystals/C, Pd/C and Pt/C electrocatalysts (Fig. 9e, f, Table 3). Moreover, the monoclinic Pd_5Bi_2 nanocrystals also display enhanced catalytic stability and maintain the highest mass activity among the catalysts after 10,000 cycles of ORR durability test, suggesting the prominent advantage of the crystal phase. Jiang and coworkers [110] fabricated fcc-FePd and face-centered tetragonal (fct)-FePd by annealing core/shell Pd/Fe_3O_4 nanoparticles and found that the fct-FePd was stronger ferromagnetic relative to fcc-FePd and exhibited higher ORR activity and stability in 0.1 $mol{\cdot}L^{-1}$ $HClO_4$ solution (Table 3). After temperature-programed Fe etching in acetic acid, core/shell fct-FePd/Pd nanoparticles (Fig. 8d) was obtained, and the performance was further enhanced.

4.4 Support effect

In the application of electrocatalysis, support materials are often used. The interaction between metal catalysts and supports would modulate the electronic structures of catalysts and boost the electrocatalytic reaction kinetics, thus help to enhance the electrocatalytic activity (Table 4) [111, 112]. In addition, the dispersity and stability of catalysts can be improved with the utilization of support materials [113]. Carbon-based materials with good electrical conductivity, high specific surface area, and affordable price, have become the most commonly used support materials [114]. For example, Zheng et al. [115] prepared a series of graphene (G) supported Cu_xPd_y nanocomposites (G-Cu_4Pd, G-Cu_3Pd, G-CuPd, G-$CuPd_3$, G-$CuPd_4$) and evaluated their ORR activities (Fig. 10a). Relative to pure Cu_xPd_y nanocrystals, G-Cu_xPd_y nanocomposites exhibit

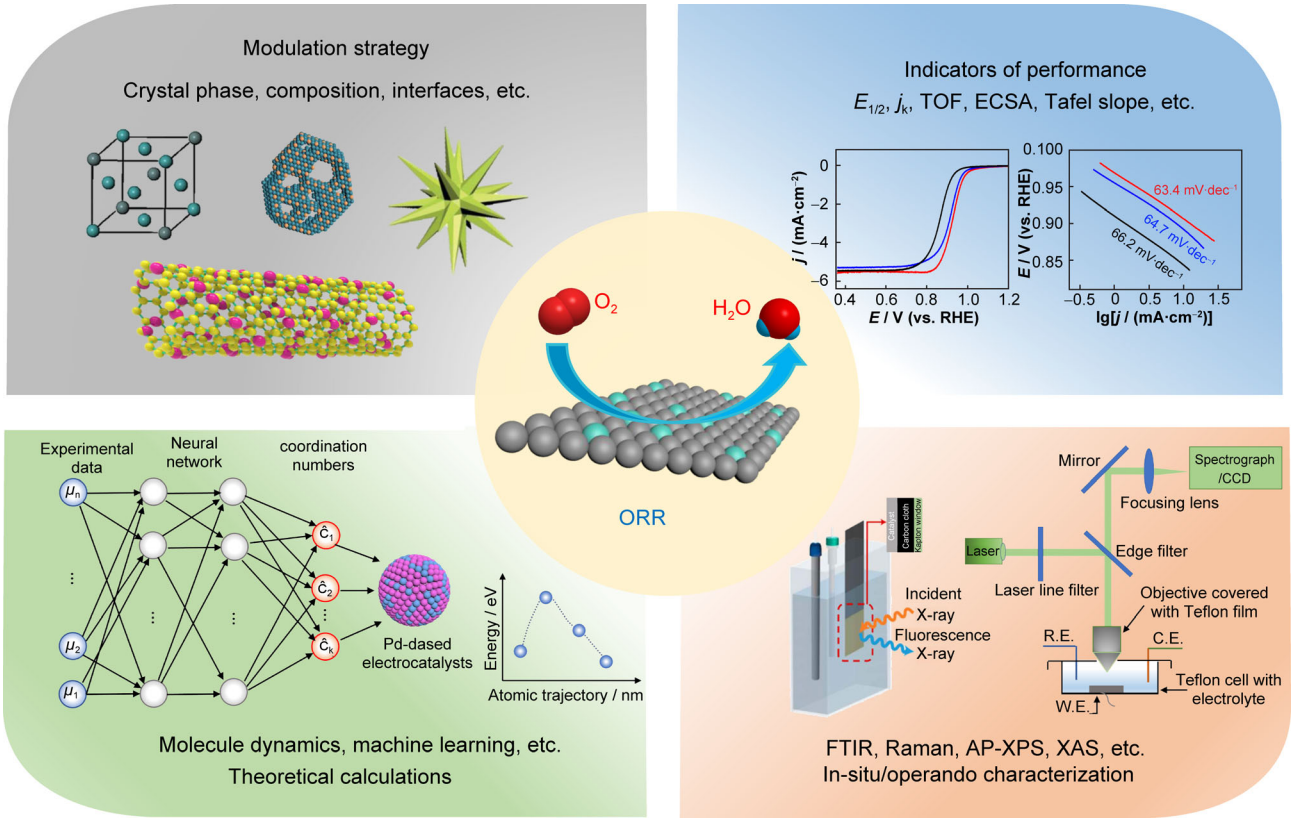

Fig. 11 An integration of synthetic strategy, performance evaluation, theoretical calculation and in situ/operando characterization for Pd-based electrocatalysts toward ORR

significantly improved interfacial electron transfer dynamics. Among them, G-Cu_3Pd nanocomposites show the best ORR electrocatalytic activity in alkaline media (Fig. 10b), which is superior to that of Pd/C catalyst and close to Pt/C catalyst. Moreover, the stability of G-Cu_3Pd could surpass that of Pt/C electrocatalyst. Such enhancement may arise from the optimized electronic structure of G-Cu_3Pd nanocomposites and the appearance of graphene. For further exploration, the ORR activities of pure G and Cu_3Pd were studied. The polarization plots suggest that G-Cu_3Pd nanocomposites exhibit more positive onset reduction potential and enhanced current density compared with pure G and Cu_3Pd. It is ascribed to the strong synergetic effect between Cu_3Pd and graphene, which accelerates interfacial electron transfer dynamics, this was also investigated by electrochemical impedance spectra. Yun et al. [116] fabricated thiolated graphene oxide-supported PdCo catalyst and found that the ORR catalytic performance was distinctly enhanced by the exposed active surface (Table 4). Li et al. [117] synthesized PdCoNi alloy nanoparticles anchored on N-doped carbon nanotubes and the obtained catalyst exhibited enhanced electrocatalytic ORR activity and stability. These results suggest that pyridine nitrogen in N-doped carbon nanotubes is beneficial to the ORR, and the stabilizing function of N-doped carbon nanotubes contributes to the improved stability.

Transition metal-based materials exhibit strong interaction with the metal catalysts and have been considered as a kind of potential support materials in electrocatalysis [122–124]. Many researches have suggested that the combination of transition metal-based materials and Pd-based nanoparticles could achieve promising ORR activity. For instance, Huang et al. [119] reported Mo_2C-coupled Pd atomic layers (AL-Pd/Mo_2C) with distinctly improved ORR activity and stability (Fig. 10c, d). Experiments and DFT calculations indicated that the Mo_2C support could affect the adjacent Pd atomic layers via the electronic effect, and optimize the d-band center of Pd atoms as well as the intermediate adsorption energy. In addition, the strong interactions between Pd metal and Mo_2C support could stabilize the high specific surface area of Pd atomic layers. Lu et al. [120] synthesized Pd hydride nanocubes embedded into 2D amorphous NiB nanosheets through a two-step method. The $PdH_{0.43}$ nanocubes were fabricated firstly and then embedded into 2D amorphous NiB nanosheets by $NaBH_4$ reduction with the presence of Ni species. In the process, $PdH_{0.43}$ would further transform

into $PdH_{0.706}$ because of the production of endogenous H_2. As seen in Fig. 10e, the obtained composites could maintain the initial shape and size of $PdH_{0.43}$ nanocubes. From the ORR polarization curves, $PdH_{0.706}$@Ni–B/C exhibits the improved activity relative to $PdH_{0.706}$/C without NiB wrap (Fig. 10f, Table 4). It is ascribed to the strong electron effect, because the BO_2^- species in NiB membrane are electron-deficient, which could effectively tune the binding energies of O and OH species, and result in an optimal value for excellent electrocatalysts for ORR. Dong et al. [113] firstly synthesized Mn_2O_3 mesoporous nanostructure as support material and then prepared Mn_2O_3-Pd nanocomposites with various Pd loading amounts. The obtained composites exhibit competitive ORR activity and selectivity to the commercial Pt/C. Both the mesoporous structure of Mn_2O_3 and the synergic effect between Pd nanoparticles and support contribute to the enhanced ORR performance.

5 Summary and outlook

Considering the low reserve and high price of Pt, Pd-based nanomaterials have been well regarded as a promising substitute of Pt in the ORR, due to the similar electronic structure of Pd and the comparable electrocatalytic performance. In this review, the recent advance of Pd-based ORR electrocatalysts is summarized, including the ORR mechanism, the synthetic methods of Pd-based nanoparticles, and the effects of composition, morphology, crystal phase and support materials of Pd-based catalysts on ORR. Pd-based nanoparticles have shown promising electrocatalytic activity towards ORR, some of which even surpass commercial Pt/C catalyst, particularly in alkaline conditions. In addition, Pd-based electrocatalysts often exhibit higher methanol tolerance relative to Pt/C, thus demonstrating great potential in ORR electrocatalysis. However, some drawbacks also exist and many issues need to be addressed in the future research.

Pd-based nanoparticles demonstrate superior ORR performance comparable to commercial Pt/C electrocatalyst in alkaline media. However, in acid solution, they often show unsatisfactory capacity and durability compared to Pt/C. Therefore, the exploration of highly active and stable Pd-based ORR electrocatalysts in acidic media is of great concern. To achieve high-performance Pd-based electrocatalysts, we think that it is an integration of the following aspects as shown in Fig. 11. Firstly, the incorporation of other metal/nonmetal elements could adjust the electronic structure of Pd, therefore, Pd-based bimetallic and multimetallic nanoparticles tend to achieving higher ORR activity relative to single Pd [125, 126]. However, in previous reports, Pd element often accounts for the main content in the nanostructures and only a small amount of non-noble metals can be incorporated. In this concern, the preparation of catalysts with increased content of transition metal or nonmetal elements is an effective strategy to prepare cost-effective electrocatalysts. In this regard, the high-entropy alloy may open a new avenue for the rational design of Pd-based electrocatalysts [127]. Secondary, the morphology and crystal phase play important roles in improving the ORR performance of Pd-based nanoparticles. Thus, precise synthesis or modulation of specific crystal plane or surface is a prerequisite for the systematic study of the relationship between morphology or crystal phase and catalytic property [34, 101]. Thirdly, the introduction of support materials would promote catalytic reaction kinetics and prevent the agglomeration of catalysts [115, 128]. Therefore, the design of adequate support materials is paramount in adjusting the interaction between the catalyst and support, which is beneficial for reducing the loading of Pd.

In addition to the design of electrocatalysts themselves, the understanding on catalytic mechanism or reaction process is equally significant. To achieve this goal, in situ or operando characterization techniques are undergoing a booming development, such as in situ/operando Fourier transform infrared spectroscopy (FTIR), X-ray absorption spectroscopy (XAS), ambient-pressure X-ray photoelectron spectroscopy (AP-XPS). [129]. Another powerful tool to reveal the intrinsic property of electrocatalysts is the theoretical calculations based on large computational power. Currently, it has become a common phenomenon to explain the underlying electrocatalytic process or mechanism by DFT and molecule dynamics. Moreover, machine learning is becoming an attractive strategy to screen a large amount of materials toward highly efficient electrocatalysts, demonstrating great prospect in saving time and lowering the cost of experiments. In summary, the development of cost-effective, environmentally friendly and durable Pd-based ORR electrocatalysts is highly desired, and concerted efforts are required to achieve great progress in the practical application in the near future.

Acknowledgements This study was financially supported by the National Natural Science Foundation of China (No. 52172058).

Declarations

Conflict of interests The authors declare that they have no conflict of interest.

References

[1] Seh ZW, Kibsgaard J, Dickens CF, Chorkendorff I, Norskov JK, Jaramillo TF. Combining theory and experiment in

electrocatalysis: insights into materials design. Science. 2017; 355(6321):eaad4998. https://doi.org/10.1126/science.aad4998.
[2] Wang C, Tian Y, Gu Y, Xue KH, Sun H, Miao X, Dai L. Plasma-induced moieties impart super-efficient activity to hydrogen evolution electrocatalysts. Nano Energy. 2021;85: 106030. https://doi.org/10.1016/j.nanoen.2021.106030.
[3] Huang C, Wang X, Wang D, Zhao W, Bu K, Xu J, Huang X, Bi Q, Huang J, Huang F. Atomic pillar effect in Pd_xNbS_2 to boost basal plane activity for stable hydrogen evolution. Chem Mater. 2019;31(13):4726. https://doi.org/10.1021/acs.chemmater.9b00821.
[4] Wang D, Wang X, Lu Y, Song C, Pan J, Li C, Sui M, Zhao W, Huang F. Atom-scale dispersed palladium in a conductive $Pd_{0.1}TaS_2$ lattice with a unique electronic structure for efficient hydrogen evolution. J Mater Chem A. 2017;5(43):22618. https://doi.org/10.1039/c7ta06447k.
[5] Zuo X, Yan R, Zhao L, Long Y, Shi L, Cheng Q, Liu D, Hu C. A hollow PdCuMoNiCo high-entropy alloy as an efficient bi-functional electrocatalyst for oxygen reduction and formic acid oxidation. J Mater Chem A. 2022;10(28):14857. https://doi.org/10.1039/d2ta02597c.
[6] Zhang W, Chang J, Wang G, Li Z, Wang M, Zhu Y, Li B, Zhou H, Wang G, Gu M, Feng Z, Yang Y. Surface oxygenation induced strong interaction between Pd catalyst and functional support for zinc-air batteries. Energy Environ Sci. 2022;15(4): 1573. https://doi.org/10.1039/d1ee03972e.
[7] Nie Y, Li L, Wei Z. Recent advancements in Pt and Pt-free catalysts for oxygen reduction reaction. Chem Soc Rev. 2015; 44(8):2168. https://doi.org/10.1039/c4cs00484a.
[8] Zhu C, Li H, Fu S, Du D, Lin Y. Highly efficient nonprecious metal catalysts towards oxygen reduction reaction based on three-dimensional porous carbon nanostructures. Chem Soc Rev. 2016;45(3):517. https://doi.org/10.1039/c5cs00670h.
[9] Yang W, Liu X, Yue X, Jia J, Guo S. Bamboo-like carbon nanotube/Fe_3C nanoparticle hybrids and their highly efficient catalysis for oxygen reduction. J Am Chem Soc. 2015;137(4): 1436. https://doi.org/10.1021/ja5129132.
[10] Huang L, Zaman S, Tian X, Wang Z, Fang W, Xia BY. Advanced platinum-based oxygen reduction electrocatalysts for fuel cells. Acc Chem Res. 2021;54(2):311. https://doi.org/10.1021/acs.accounts.0c00488.
[11] Ma Z, Cano ZP, Yu A, Chen Z, Jiang G, Fu X, Yang L, Wu T, Bai Z, Lu J. Enhancing oxygen reduction activity of Pt-based electrocatalysts: from theoretical mechanisms to practical methods. Angew Chem Int Ed. 2020;59(42):18334. https://doi.org/10.1002/anie.202003654.
[12] Dai L, Xue Y, Qu L, Choi HJ, Baek JB. Metal-free catalysts for oxygen reduction reaction. Chem Rev. 2015;115(11):4823. https://doi.org/10.1021/cr5003563.
[13] Zhu C, Shi Q, Xu BZ, Fu S, Wan G, Yang C, Yao S, Song J, Zhou H, Du D, Beckman SP, Su D, Lin Y. Hierarchically porous M-N-C (M=Co and Fe) single-atom electrocatalysts with robust MN_x active moieties enable enhanced ORR performance. Adv Energy Mater. 2018;8(29):1801956. https://doi.org/10.1002/aenm.201801956.
[14] Xue Q, Xu G, Mao R, Liu H, Zeng J, Jiang J, Chen Y. Polyethyleneimine modified AuPd@PdAu alloy nanocrystals as advanced electrocatalysts towards the oxygen reduction reaction. J Energ Chem. 2017;26(6):1153. https://doi.org/10.1016/j.jechem.2017.06.007.
[15] Luo JY, Han PP, Dan ZH, Tang T, Qin FX, Chang H, Zhou L. Electrocatalytic oxygen reduction performances of surface Ag granular packs electrodeposited from dual-phase $Ag_{35.5}Zn_{64.5}$ precursor alloys by triangle wave potential cycling. Rare Met. 2021;40(12):3531. https://doi.org/10.1007/s12598-020-01700-1.
[16] Liang Y, Wang H, Diao P, Chang W, Hong G, Li Y, Gong M, Xie L, Zhou J, Wang J, Regier TZ, Wei F, Dai H. Oxygen reduction electrocatalyst based on strongly coupled cobalt oxide nanocrystals and carbon nanotubes. J Am Chem Soc. 2012;134(38):15849. https://doi.org/10.1021/ja305623m.
[17] Li Z, Wei L, Jiang WJ, Hu Z, Luo H, Zhao W, Xu T, Wu W, Wu M, Hu JS. Chemical state of surrounding iron species affects the activity of Fe–N_x for electrocatalytic oxygen reduction. Appl Catal B Environ. 2019;251:240. https://doi.org/10.1016/j.apcatb.2019.03.046.
[18] Zhang J, Zhang C, Zhao Y, Amiinu IS, Zhou H, Liu X, Tang Y, Mu S. Three dimensional few-layer porous carbon nanosheets towards oxygen reduction. Appl Catal B Environ. 2017;211: 148. https://doi.org/10.1016/j.apcatb.2017.04.038.
[19] Rybarczyk MK, Gontarek E, Lieder M, Titirici MM. Salt melt synthesis of curved nitrogen-doped carbon nanostructures: ORR kinetics boost. Appl Surf Sci. 2018;435:543. https://doi.org/10.1016/j.apsusc.2017.11.064.
[20] Lin Z, Yang A, Zhang B, Liu B, Zhu J, Tang Y, Qiu X. Coupling the atomically dispersed Fe–N_3 sites with sub-5 nm Pd nanocrystals confined in N-doped carbon nanobelts to boost the oxygen reduction for microbial fuel cells. Adv Funct Mater. 2021. https://doi.org/10.1002/adfm.202107683.
[21] Si W, Yang Z, Hu X, Lv Q, Li X, Zhao F, He J, Huang C. Preparation of zero valence Pd nanoparticles with ultra-efficient electrocatalytic activity for ORR. J Mater Chem A. 2021; 9(25):14507. https://doi.org/10.1039/d1ta00788b.
[22] Chen A, Ostrom C. Palladium-based nanomaterials: synthesis and electrochemical applications. Chem Rev. 2015;115(21): 11999. https://doi.org/10.1021/acs.chemrev.5b00324.
[23] Wang T, Chutia A, Brett DJL, Shearing PR, He G, Chai G, Parkin IP. Palladium alloys used as electrocatalysts for the oxygen reduction reaction. Energy Environ Sci. 2021;14(5): 2639. https://doi.org/10.1039/d0ee03915b.
[24] Shao M, Chang Q, Dodelet JP, Chenitz R. Recent advances in electrocatalysts for oxygen reduction reaction. Chem Rev. 2016;116(6):3594. https://doi.org/10.1021/acs.chemrev.5b00462.
[25] Yang Y, Chen G, Zeng R, Villarino AM, DiSalvo FJ, van Dover RB, Abruna HD. Combinatorial studies of palladium-based oxygen reduction electrocatalysts for alkaline fuel cells. J Am Chem Soc. 2020;142(8):3980. https://doi.org/10.1021/jacs.9b13400.
[26] Li Y, Lin S, Ren X, Mi H, Zhang P, Sun L, Deng L, Gao Y. One-step rapid in-situ synthesis of nitrogen and sulfur co-doped three-dimensional honeycomb-ordered carbon supported PdNi nanoparticles as efficient electrocatalyst for oxygen reduction reaction in alkaline solution. Electrochim Acta. 2017;253:445. https://doi.org/10.1016/j.electacta.2017.08.143.
[27] Liu Z, Yang X, Lu B, Shi Z, Sun D, Xu L, Tang Y, Sun S. Delicate topotactic conversion of coordination polymers to Pd porous nanosheets for high-efficiency electrocatalysis. Appl Catal B Environ. 2019;243:86. https://doi.org/10.1016/j.apcatb.2018.10.028.
[28] Duan H, Xu C. Nanoporous PdCr alloys as highly active electrocatalysts for oxygen reduction reaction. Phys Chem Chem Phys. 2016;18(5):4166. https://doi.org/10.1039/c5cp07184d.
[29] Wang H, Yin S, Li Y, Yu H, Li C, Deng K, Xu Y, Li X, Xue H, Wang L. One-step fabrication of tri-metallic PdCuAu nanothorn assemblies as an efficient catalyst for oxygen reduction reaction. J Mater Chem A. 2018;6(8):3642. https://doi.org/10.1039/c7ta10342e.
[30] Mahata A, Nair AS, Pathak B. Recent advancements in Pt-nanostructure-based electrocatalysts for the oxygen

reduction reaction. Catal Sci Technol. 2019;9(18):4835. https://doi.org/10.1039/c9cy00895k.
[31] Slanac DA, Hardin WG, Johnston KP, Stevenson KJ. Atomic ensemble and electronic effects in Ag-rich AgPd nanoalloy catalysts for oxygen reduction in alkaline media. J Am Chem Soc. 2012;134(23):9812. https://doi.org/10.1021/ja303580b.
[32] Srejic I, Rakocevic Z, Nenadovic M, Strbac S. Oxygen reduction on polycrystalline palladium in acid and alkaline solutions: topographical and chemical Pd surface changes. Electrochim Acta. 2015;169:22. https://doi.org/10.1016/j.electacta.2015.04.032.
[33] Naik KM, Hashisake K, Hamada T, Higuchi E, Inoue H. Intermetallic PdZn nanoparticles loaded on deficient TiO_2 nanosheets as a support: a bifunctional electrocatalyst for oxygen reduction in PEMFCs and the glycerol oxidation reactions. J Mater Chem A. 2022;10(26):13987. https://doi.org/10.1039/d2ta03736j.
[34] Yu Z, Xu S, Feng Y, Yang C, Yao Q, Shao Q, Li YF, Huang X. Phase-controlled synthesis of Pd-Se nanocrystals for phase-dependent oxygen reduction catalysis. Nano Lett. 2021;21(9):3805. https://doi.org/10.1021/acs.nanolett.1c00147.
[35] Li L, He J, Wang Y, Lv X, Gu X, Dai P, Liu D, Zhao X. Metal-organic frameworks: a promising platform for constructing non-noble electrocatalysts for the oxygen-reduction reaction. J Mater Chem A. 2019;7(5):1964. https://doi.org/10.1039/c8ta11704g.
[36] Nørskov JK, Rossmeisl J, Logadottir A, Lindqvist L. Origin of the overpotential for oxygen reduction at a fuel-cell cathode. J Phys Chem B. 2004;108:17886. https://doi.org/10.1021/jp047349j.
[37] Ma R, Lin G, Zhou Y, Liu Q, Zhang T, Shan G, Yang M, Wang J. A review of oxygen reduction mechanisms for metal-free carbon-based electrocatalysts. NPJ Comput Mater. 2019;5(1):78. https://doi.org/10.1038/s41524-019-0210-3.
[38] Li C, Zhao DH, Long HL, Li M. Recent advances in carbonized non-noble metal–organic frameworks for electrochemical catalyst of oxygen reduction reaction. Rare Met. 2021;40(10):2657. https://doi.org/10.1007/s12598-020-01694-w.
[39] Risch M. Perovskite electrocatalysts for the oxygen reduction reaction in alkaline media. Catalysts. 2017;7(5):154. https://doi.org/10.3390/catal7050154.
[40] Zagal JH, Specchia S, Atanassov P. Mapping transition metal-MN_4 macrocyclic complex catalysts performance for the critical reactivity descriptors. Curr Opin Electrochem. 2021;27:100683. https://doi.org/10.1016/j.coelec.2020.100683.
[41] Zhao Z, Chen C, Liu Z, Huang J, Wu M, Liu H, Li Y, Huang Y. Pt-based nanocrystal for electrocatalytic oxygen reduction. Adv Mater. 2019;31(31):1808115. https://doi.org/10.1002/adma.201808115.
[42] Liu M, Zhao Z, Duan X, Huang Y. Nanoscale structure design for high-performance Pt-based ORR catalysts. Adv Mater. 2019;31(6):1802234. https://doi.org/10.1002/adma.201802234.
[43] Kakaei K, Dorraji M. One-pot synthesis of palladium silver nanoparticles decorated reduced graphene oxide and their application for ethanol oxidation in alkaline media. Electrochim Acta. 2014;143:207. https://doi.org/10.1016/j.electacta.2014.07.134.
[44] Fu S, Zhu C, Du D, Lin Y. Facile one-step synthesis of three-dimensional Pd-Ag bimetallic alloy networks and their electrocatalytic activity toward ethanol oxidation. ACS Appl Mater Interfaces. 2015;7(25):13842. https://doi.org/10.1021/acsami.5b01963.
[45] Wang H, Li Y, Li C, Wang Z, Xu Y, Li X, Xue H, Wang L. Hyperbranched PdRu nanospine assemblies: an efficient electrocatalyst for formic acid oxidation. J Mater Chem A. 2018;6(36):17514. https://doi.org/10.1039/c8ta06908e.
[46] Zhang Z, Wang Z, He S, Wang C, Jin M, Yin Y. Redox reaction induced Ostwald ripening for size- and shape-focusing of palladium nanocrystals. Chem Sci. 2015;6(9):5197. https://doi.org/10.1039/c5sc01787d.
[47] Zhang J, Xu Y, Zhang B. Facile synthesis of 3D Pd–P nanoparticle networks with enhanced electrocatalytic performance towards formic acid electrooxidation. Chem Commun. 2014;50(88):13451. https://doi.org/10.1039/c4cc03282a.
[48] Zareie Yazdan-Abad M, Noroozifar M, Modaresi Alam AR, Saravani H. Palladium aerogel as a high-performance electrocatalyst for ethanol electro-oxidation in alkaline media. J Mater Chem A. 2017;5(21):10244. https://doi.org/10.1039/c7ta03208k.
[49] Jiang B, Zhang XG, Jiang K, Wu DY, Cai WB. Boosting formate production in electrocatalytic CO_2 reduction over wide potential window on Pd surfaces. J Am Chem Soc. 2018;140(8):2880. https://doi.org/10.1021/jacs.7b12506.
[50] Zhu C, Shi Q, Fu S, Song J, Du D, Su D, Engelhard MH, Lin Y. Core-shell PdPb@Pd aerogels with multiply-twinned intermetallic nanostructures: facile synthesis with accelerated gelation kinetics and their enhanced electrocatalytic properties. J Mater Chem A. 2018;6(17):7517. https://doi.org/10.1039/c7ta11233e.
[51] Huang X, Li Y, Chen Y, Zhou E, Xu Y, Zhou H, Duan X, Huang Y. Palladium-based nanostructures with highly porous features and perpendicular pore channels as enhanced organic catalysts. Angew Chem Int Ed. 2013;52(9):2520. https://doi.org/10.1002/anie.201208901.
[52] Li C, Iqbal M, Jiang B, Wang Z, Kim J, Nanjundan AK, Whitten AE, Wood K, Yamauchi Y. Pore-tuning to boost the electrocatalytic activity of polymeric micelle-templated mesoporous Pd nanoparticles. Chem Sci. 2019;10(14):4054. https://doi.org/10.1039/c8sc03911a.
[53] Choi S, Jeong H, Choi KH, Song JY, Kim J. Electrodeposition of triangular Pd rod nanostructures and their electrocatalytic and SERS activities. ACS Appl Mater Interfaces. 2014;6(4):3002. https://doi.org/10.1021/am405601g.
[54] Xu D, Yan X, Diao P, Yin P. Electrodeposition of vertically aligned palladium nanoneedles and their application as active substrates for surface-enhanced raman scattering. J Phys Chem C. 2014;118(18):9758. https://doi.org/10.1021/jp500667f.
[55] Li YF, Lv JJ, Zhang M, Feng JJ, Li FF, Wang AJ. A simple and controlled electrochemical deposition route to urchin-like Pd nanoparticles with enhanced electrocatalytic properties. J Electroanal Chem. 2015;738:1. https://doi.org/10.1016/j.jelechem.2014.11.017.
[56] Duan J, Lyu S, Yao H, Mo D, Chen Y, Sun Y, Maaz K, Maqbool M, Liu J. Controlled structure of electrochemically deposited Pd nanowires in ion-track templates. Nanoscale Res Lett. 2015;10(1):481. https://doi.org/10.1186/s11671-015-1189-4.
[57] Das AK, Kim NH, Pradhan D, Hui D, Lee JH. Electrochemical synthesis of palladium (Pd) nanorods: an efficient electrocatalyst for methanol and hydrazine electro-oxidation. Compos Part B Eng. 2018;144:11. https://doi.org/10.1016/j.compositesb.2018.02.017.
[58] Fang Y, Guo S, Zhu C, Dong S, Wang E. Twenty second synthesis of pd nanourchins with high electrochemical activity through an electrochemical route. Langmuir. 2010;26(23):17816. https://doi.org/10.1021/la1036597.
[59] Jeong H, Kim J. Electrodeposition of nanoflake Pd structures: structure-dependent wettability and SERS activity. ACS Appl Mater Interfaces. 2015;7(13):7129. https://doi.org/10.1021/acsami.5b02113.

[60] Jia F, Wong KW, Du R. Direct growth of highly catalytic palladium nanoplates array onto gold substrate by a template-free electrochemical route. Electrochem Commun. 2009; 11(3):519. https://doi.org/10.1016/j.elecom.2008.11.054.
[61] Xu CW, Wang H, Shen PK, Jiang SP. Highly ordered Pd nanowire arrays as effective electrocatalysts for ethanol oxidation in direct alcohol fuel cells. Adv Mater. 2007;19(23): 4256. https://doi.org/10.1002/adma.200602911.
[62] Zhao Y, Qin SJ, Li Y, Deng FX, Liu YQ, Pan GB. Electrodeposition of dendritic Pd nanoarchitectures on n-GaN(0001): nucleation and electrocatalysis for direct formic acid fuel cells. Electrochim Acta. 2014;145:148. https://doi.org/10.1016/j.electacta.2014.09.008.
[63] Su Y, Prestat E, Hu C, Puthiyapura VK, Neek-Amal M, Xiao H, Huang K, Kravets VG, Haigh SJ, Hardacre C, Peeters FM, Nair RR. Self-limiting growth of two-dimensional palladium between graphene oxide layers. Nano Lett. 2019;19(7):4678. https://doi.org/10.1021/acs.nanolett.9b01733.
[64] Li C, Jiang B, Miyamoto N, Kim JH, Malgras V, Yamauchi Y. Surfactant-directed synthesis of mesoporous Pd films with perpendicular mesochannels as efficient electrocatalysts. J Am Chem Soc. 2015;137(36):11558. https://doi.org/10.1021/jacs.5b06278.
[65] Iqbal M, Kim J, Yuliarto B, Jiang B, Li C, Dag O, Malgras V, Yamauchi Y. Standing mesochannels: mesoporous PdCu films with vertically aligned mesochannels from nonionic micellar solutions. ACS Appl Mater Interfaces. 2018;10(47):40623. https://doi.org/10.1021/acsami.8b13662.
[66] An Y, Tian Y, Wei C, Tao Y, Xi B, Xiong S, Feng J, Qian Y. Dealloying: an effective method for scalable fabrication of 0D, 1D, 2D, 3D materials and its application in energy storage. Nano Today. 2021;37:101094. https://doi.org/10.1016/j.nantod.2021.101094.
[67] Fujita T. Hierarchical nanoporous metals as a path toward the ultimate three-dimensional functionality. Sci Technol Adv Mater. 2017;18(1):724. https://doi.org/10.1080/14686996.2017.1377047.
[68] Liu Y, Xu C. Nanoporous PdTi alloys as non-platinum oxygen-reduction reaction electrocatalysts with enhanced activity and durability. Chemsuschem. 2013;6(1):78. https://doi.org/10.1002/cssc.201200752.
[69] Chen J, Li Y, Lu N, Tian C, Han Z, Zhang L, Fang Y, Qian B, Jiang X, Cui R. Nanoporous PdCe bimetallic nanocubes with high catalytic activity towards ethanol electro-oxidation and the oxygen reduction reaction in alkaline media. J Mater Chem A. 2018;6(46):23560. https://doi.org/10.1039/c8ta08445a.
[70] Sun D, Wang Y, Livi KJT, Wang C, Luo R, Zhang Z, Alghamdi H, Li C, An F, Gaskey B, Mueller T, Hall AS. Ordered intermetallic Pd_3Bi prepared by an electrochemically induced phase transformation for oxygen reduction electrocatalysis. ACS Nano. 2019;13(9):10818. https://doi.org/10.1021/acsnano.9b06019.
[71] Lu X, Ahmadi M, DiSalvo FJ, Abruña HD. Enhancing the electrocatalytic activity of Pd/M (M=Ni, Mn) nanoparticles for the oxygen reduction reaction in alkaline media through electrochemical dealloying. ACS Catal. 2020;10(10):5891. https://doi.org/10.1021/acscatal.9b05499.
[72] Shi S, Markmann J, Weissmüller J. Synthesis of uniform bulk nanoporous palladium with tunable structure. Electrochim Acta. 2018;285:60. https://doi.org/10.1016/j.electacta.2018.07.081.
[73] Gunji T, Wakabayashi RH, Noh SH, Han B, Matsumoto F, DiSalvo FJ, Abruña HD. The effect of alloying of transition metals (M=Fe Co, Ni) with palladium catalysts on the electrocatalytic activity for the oxygen reduction reaction in alkaline media. Electrochim Acta. 2018;283:1045. https://doi.org/10.1016/j.electacta.2018.06.051.
[74] Zhang M, Li MP, Yin T, Zhang T. Fabrication of nanoporous bi-metallic Ag-Pd alloys with open pores. Mater Lett. 2016; 162:273. https://doi.org/10.1016/j.matlet.2015.10.014.
[75] Song Y, Zhang X, Yang S, Wei X, Sun Z. Electrocatalytic performance for methanol oxidation on nanoporous Pd/NiO composites prepared by one-step dealloying. Fuel. 2016;181: 269. https://doi.org/10.1016/j.fuel.2016.04.086.
[76] Lim MB, Hanson JL, Vandsburger L, Roder PB, Zhou X, Smith BE, Ohuchi FS, Pauzauskie PJ. Copper- and chloride-mediated synthesis and optoelectronic trapping of ultra--high aspect ratio palladium nanowires. J Mater Chem A. 2018; 6(14):5644. https://doi.org/10.1039/c7ta07324k.
[77] Kong Q, Feng W, Zhong X, Liu Y, Lian L. Hydrogen absorption/desorption properties of porous hollow palladium spheres prepared by templating method. J Alloys Compd. 2016; 664:188. https://doi.org/10.1016/j.jallcom.2015.12.234.
[78] Li R, Zhang P, Huang Y, Chen C, Chen Q. Facile approach to prepare Pd nanoarray catalysts within porous alumina templates on macroscopic scales. ACS Appl Mater Interfaces. 2013;5(23):12695. https://doi.org/10.1021/am4040762.
[79] Chen D, Sun P, Liu H, Yang J. Bimetallic Cu-Pd alloy multipods and their highly electrocatalytic performance for formic acid oxidation and oxygen reduction. J Mater Chem A. 2017; 5(9):4421. https://doi.org/10.1039/c6ta10476b.
[80] Sanij FD, Balakrishnan P, Leung P, Shah A, Su H, Xu Q. Advanced Pd-based nanomaterials for electro-catalytic oxygen reduction in fuel cells: a review. Int J Hydrogen Energ. 2021; 46(27):14596. https://doi.org/10.1016/j.ijhydene.2021.01.185.
[81] Zong Z, Xu K, Li D, Tang Z, He W, Liu Z, Wang X, Tian Y. Peptide templated Au@Pd core-shell structures as efficient bi-functional electrocatalysts for both oxygen reduction and hydrogen evolution reactions. J Catal. 2018;361:168. https://doi.org/10.1016/j.jcat.2018.02.020.
[82] Nguyen ATN, Shim JH. Facile one-step synthesis of Ir–Pd bimetallic alloy networks as efficient bifunctional catalysts for oxygen reduction and oxygen evolution reactions. J Electroanal Chem. 2018;827:120. https://doi.org/10.1016/j.jelechem.2018.09.012.
[83] Wang H, Zhou T, Deng K, Jiao S, Tian W, Xu Y, Li X, Wang Z, Wang L. Mesoporous PdRu nanocrystals for oxygen reduction electrocatalysis. Energy Fuels. 2021;35(16):13382. https://doi.org/10.1021/acs.energyfuels.1c01658.
[84] Yan Y, Zhan F, Du J, Jiang Y, Jin C, Fu M, Zhang H, Yang D. Kinetically-controlled growth of cubic and octahedral Rh-Pd alloy oxygen reduction electrocatalysts with high activity and durability. Nanoscale. 2015;7(1):301. https://doi.org/10.1039/c4nr04942j.
[85] Xie Y, Li C, Castillo E, Fang J, Dimitrov N. Nanoporous Pd-Cu thin films as highly active and durable catalysts for oxygen reduction in alkaline media. Electrochim Acta. 2021; 385: 138306. https://doi.org/10.1016/j.electacta.2021.138306.
[86] Sun L, Liao B, Ren X, Li Y, Zhang P, Deng L, Gao Y. Ternary PdNi-based nanocrystals supported on nitrogen-doped reduced graphene oxide as highly active electrocatalysts for the oxygen reduction reaction. Electrochim Acta. 2017;235:543. https://doi.org/10.1016/j.electacta.2017.03.159.
[87] Liu S, Xiao W, Wang J, Zhu J, Wu Z, Xin H, Wang D. Ultralow content of Pt on Pd-Co-Cu/C ternary nanoparticles with excellent electrocatalytic activity and durability for the oxygen reduction reaction. Nano Energy. 2016;27:475. https://doi.org/10.1016/j.nanoen.2016.07.038.
[88] Zhao F, Zheng L, Yuan Q, Yang X, Zhang Q, Xu H, Guo Y, Yang S, Zhou Z, Gu L, Wang X. Ultrathin PdAuBiTe nanosheets as high-performance oxygen reduction catalysts for

a direct methanol fuel cell device. Adv Mater. 2021;33(42): 2103383. https://doi.org/10.1002/adma.202103383.
[89] Yang Y, Xiao W, Feng X, Xiong Y, Gong M, Shen T, Lu Y, Abruna HD, Wang D. Golden palladium zinc ordered intermetallics as oxygen reduction electrocatalysts. ACS Nano. 2019;13(5):5968. https://doi.org/10.1021/acsnano.9b01961.
[90] Guo J, Gao L, Tan X, Yuan Y, Kim J, Wang Y, Wang H, Zeng YJ, Choi SI, Smith SC, Huang H. Template-directed rapid synthesis of Pd-based ultrathin porous intermetallic nanosheets for efficient oxygen reduction. Angew Chem Int Ed. 2021; 60(19):10942. https://doi.org/10.1002/anie.202100307.
[91] Du C, Li P, Yang F, Cheng G, Chen S, Luo W. Monodisperse palladium sulfide as efficient electrocatalyst for oxygen reduction reaction. ACS Appl Mater Interfaces. 2018;10(1): 753. https://doi.org/10.1021/acsami.7b16359.
[92] Vo Doan TT, Wang J, Poon KC, Tan DC, Khezri B, Webster RD, Su H, Sato H. Theoretical modelling and facile synthesis of a highly active boron-doped palladium catalyst for the oxygen reduction reaction. Angew Chem Int Ed. 2016;55(24): 6842. https://doi.org/10.1002/anie.201601727.
[93] Lüsi M, Erikson H, Piirsoo H-M, Paiste P, Aruväli J, Kikas A, Kisand V, Tamm A, Tammeveski K. Oxygen reduction reaction on PdM/C (M=Pb, Sn, Bi) alloy nanocatalysts. J Electroanal Chem. 2022;917:116391. https://doi.org/10.1016/j.jelechem.2022.116391.
[94] Liu D, Zeng Q, Hu C, Liu H, Chen D, Han Y, Xu L, Yang J. Core-shell CuPd@NiPd nanoparticles: coupling lateral strain with electronic interaction toward high-efficiency electrocatalysis. ACS Catal. 2022;12(15):9092. https://doi.org/10.1021/acscatal.2c02274.
[95] Rego R, Ferraria AM, Botelho do Rego AM, Oliveira MC. Development of PdP nano electrocatalysts for oxygen reduction reaction. Electrochim Acta. 2013;87:73. https://doi.org/10.1016/j.electacta.2012.08.107.
[96] Li C, Chai OJH, Yao Q, Liu Z, Wang L, Wang H, Xie J. Electrocatalysis of gold-based nanoparticles and nanoclusters. Mater Horiz. 2021;8(6):1657. https://doi.org/10.1039/d0mh01947j.
[97] Huang S, Lu S, Hu H, Xu F, Li H, Duan F, Zhu H, Gu H, Du M. Hyper-dendritic PdZn nanocrystals as highly stable and efficient bifunctional electrocatalysts towards oxygen reduction and ethanol oxidation. Chem Eng J. 2021;420:130503. https://doi.org/10.1016/j.cej.2021.130503.
[98] Shi Q, Zhu C, Bi C, Xia H, Engelhard MH, Du D, Lin Y. Intermetallic Pd_3Pb nanowire networks boost ethanol oxidation and oxygen reduction reactions with significantly improved methanol tolerance. J Mater Chem A. 2017;5(45):23952. https://doi.org/10.1039/c7ta08407b.
[99] Liu Z, Yang X, Cui L, Shi Z, Lu B, Guo X, Zhang J, Xu L, Tang Y, Xiang Y. High-performance oxygen reduction electrocatalysis enabled by 3D PdNi nanocorals with hierarchical porosity. Part Part Syst Charact. 2018;35(5):1700366. https://doi.org/10.1002/ppsc.201700366.
[100] Erikson H, Sarapuu A, Alexeyeva N, Tammeveski K, Solla--Gullón J, Feliu JM. Electrochemical reduction of oxygen on palladium nanocubes in acid and alkaline solutions. Electrochim Acta. 2012;59:329. https://doi.org/10.1016/j.electacta.2011.10.074.
[101] Yu H, Zhou T, Wang Z, Xu Y, Li X, Wang L, Wang H. Defect-rich porous palladium metallene for enhanced alkaline oxygen reduction electrocatalysis. Angew Chem Int Ed. 2021; 133(21):12134. https://doi.org/10.1002/anie.202101019.
[102] Zhang Y, Huang B, Shao Q, Feng Y, Xiong L, Peng Y, Huang X. Defect engineering of palladium-tin nanowires enables efficient electrocatalysts for fuel cell reactions. Nano Lett. 2019;19(10):6894. https://doi.org/10.1021/acs.nanolett.9b02137.
[103] Liang J, Li S, Chen Y, Liu X, Wang T, Han J, Jiao S, Cao R, Li Q. Ultrathin and defect-rich intermetallic Pd_2Sn nanosheets for efficient oxygen reduction electrocatalysis. J Mater Chem A. 2020;8(31):15665. https://doi.org/10.1039/d0ta01767a.
[104] Gao F, Li C, Ren Y, Li B, Lv C, Yang X, Zhang X, Lu Z, Yu X, Li L. High-efficient ultrathin PdCuMo porous nanosheets with abundant defects for oxygen reduction reaction. Chem Eur J. 2022. https://doi.org/10.1002/chem.202201860.
[105] Liu S, Ren H, Yin S, Zhang H, Wang Z, Xu Y, Li X, Wang L, Wang H. Defect-rich ultrathin AuPd nanowires with Boerdijk–Coxeter structure for oxygen reduction electrocatalysis. Chem Eng J. 2022;435: 134823. https://doi.org/10.1016/j.cej.2022.134823.
[106] Luo M, Sun Y, Wang L, Guo S. Tuning multimetallic ordered intermetallic nanocrystals for efficient energy electrocatalysis. Adv Energy Mater. 2017;7(11):1602073. https://doi.org/10.1002/aenm.201602073.
[107] Cheng H, Yang N, Lu Q, Zhang Z, Zhang H. Syntheses and properties of metal nanomaterials with novel crystal phases. Adv Mater. 2018;30(26):1707189. https://doi.org/10.1002/adma.201707189.
[108] Ge Y, Wang X, Huang B, Huang Z, Chen B, Ling C, Liu J, Liu G, Zhang J, Wang G, Chen Y, Li L, Liao L, Wang L, Yun Q, Lai Z, Lu S, Luo Q, Wang J, Zheng Z, Zhang H. Seeded synthesis of unconventional 2H-phase Pd alloy nanomaterials for highly efficient oxygen reduction. J Am Chem Soc. 2021; 143(41):17292. https://doi.org/10.1021/jacs.1c08973.
[109] Zhou M, Guo J, Zhao B, Li C, Zhang L, Fang J. Improvement of oxygen reduction performance in alkaline media by tuning phase structure of Pd–Bi nanocatalysts. J Am Chem Soc. 2021; 143(38):15891. https://doi.org/10.1021/jacs.1c08644.
[110] Jiang G, Zhu H, Zhang X, Shen B, Wu L, Zhang S, Lu G, Wu Z, Sun S. Core/shell face-centered tetragonal FePd/Pd nanoparticles as an efficient non-Pt catalyst for the oxygen reduction reaction. ACS Nano. 2015;9:11014.
[111] Huang C, Dong W, Dong C, Wang X, Jia B, Huang F. Niobium dioxide prepared by a novel La-reduced route as a promising catalyst support for Pd towards the oxygen reduction reaction. Dalton Trans. 2020;49(5):1398. https://doi.org/10.1039/c9dt04570h.
[112] Yuan X, Wang X, Liu X, Ge H, Yin G, Dong C, Huang F. Ti^{3+}-promoted high oxygen-reduction activity of Pd nanodots supported by black titania nanobelts. ACS Appl Mater Interfaces. 2016;8(41):27654. https://doi.org/10.1021/acsami.6b07062.
[113] Dong HQ, Chen YY, Han M, Li SL, Zhang J, Li JS, Lan YQ, Dai ZH, Bao JC. Synergistic effect of mesoporous Mn_2O_3-supported Pd nanoparticle catalysts for electrocatalytic oxygen reduction reaction with enhanced performance in alkaline medium. J Mater Chem A. 2014;2(5):1272. https://doi.org/10.1039/c3ta13585c.
[114] Erikson H, Sarapuu A, Solla-Gullón J, Tammeveski K. Recent progress in oxygen reduction electrocatalysis on Pd-based catalysts. J Electroanal Chem. 2016;780:327. https://doi.org/10.1016/j.jelechem.2016.09.034.
[115] Zheng Y, Zhao S, Liu S, Yin H, Chen YY, Bao J, Han M, Dai Z. Component-controlled synthesis and assembly of Cu-Pd nanocrystals on graphene for oxygen reduction reaction. ACS Appl Mater Interfaces. 2015;7(9):5347. https://doi.org/10.1021/acsami.5b01541.
[116] Yun M, Ahmed MS, Jeon S. Thiolated graphene oxide-supported palladium cobalt alloyed nanoparticles as high performance electrocatalyst for oxygen reduction reaction. J Power

Sources. 2015;293:380. https://doi.org/10.1016/j.jpowsour.2015.05.094.
[117] Li Z, Li J, Jiang K, Yuan S, Yu D, Wei H, Shi Z, Li X, Chu H. PdCoNi alloy nanoparticles decorated, nitrogen-doped carbon nanotubes for highly active and durable oxygen reduction electrocatalysis. Chem Eng J. 2021;411:128527. https://doi.org/10.1016/j.cej.2021.128527.
[118] Chao G, Zhang L, Xue T, Tian J, Fan W, Liu T. Lattice-strain and electron-density modulation of palladium nanocatalysts for highly efficient oxygen reduction. J Colloid Interface Sci. 2021;602:159. https://doi.org/10.1016/j.jcis.2021.05.177.
[119] Huang L, Zheng X, Gao G, Zhang H, Rong K, Chen J, Liu Y, Zhu X, Wu W, Wang Y, Wang J, Dong S. Interfacial electron engineering of palladium and molybdenum carbide for highly efficient oxygen reduction. J Am Chem Soc. 2021;143(18):6933. https://doi.org/10.1021/jacs.1c00656.
[120] Lu Y, Wang J, Peng Y, Fisher A, Wang X. Highly efficient and durable pd hydride nanocubes embedded in 2D amorphous NiB nanosheets for oxygen reduction reaction. Adv Energy Mater. 2017;7(21):1700919. https://doi.org/10.1002/aenm.201700919.
[121] Karuppasamy L, Gurusamy L, Anandan S, Liu CH, Wu JJ. Defect-enriched heterointerfaces N-MoO_2-Mo_2C supported Pd nanocomposite as a novel multifunctional electrocatalyst for oxygen reduction reaction and overall water splitting. Mater Today Chem. 2022;24:100799. https://doi.org/10.1016/j.mtchem.2022.100799.
[122] Choi CH, Park SH, Woo SI. Oxygen reduction activity of Pd–Mn_3O_4 nanoparticles and performance enhancement by voltammetrically accelerated degradation. Phys Chem Chem Phys. 2012;14(19):6842. https://doi.org/10.1039/c2cp24128e.
[123] Sun H, Tung CW, Qiu Y, Zhang W, Wang Q, Li Z, Tang J, Chen HC, Wang C, Chen HM. Atomic metal-support interaction enables reconstruction-free dual-site electrocatalyst. J Am Chem Soc. 2022;144(3):1174. https://doi.org/10.1021/jacs.1c08890.
[124] Chen B, Humayun M, Li Y, Zhang H, Sun H, Wu Y, Wang C. Constructing hierarchical fluffy CoO-Co_4N@NiFe-LDH nanorod arrays for highly effective overall water splitting and urea electrolysis. ACS Sustain Chem Eng. 2021;9(42):14180. https://doi.org/10.1021/acssuschemeng.1c04674.
[125] Xiao W, Cordeiro MAL, Gao G, Zheng A, Wang J, Lei W, Gong M, Lin R, Stavitski E, Xin HL, Wang D. Atomic rearrangement from disordered to ordered Pd–Fe nanocatalysts with trace amount of Pt decoration for efficient electrocatalysis. Nano Energy. 2018;50:70. https://doi.org/10.1016/j.nanoen.2018.05.032.
[126] Maiti K, Balamurugan J, Peera SG, Kim NH, Lee JH. Highly active and durable core-shell fct-PdFe@Pd nanoparticles encapsulated ng as an efficient catalyst for oxygen reduction reaction. ACS Appl Mater Interfaces. 2018;10(22):18734. https://doi.org/10.1021/acsami.8b04060.
[127] Batchelor TAA, Pedersen JK, Winther SH, Castelli IE, Jacobsen KW, Rossmeisl J. High-entropy alloys as a discovery platform for electrocatalysis. Joule. 2019;3(3):834. https://doi.org/10.1016/j.joule.2018.12.015.
[128] Guo Y, Zhang L, XiLi D, Kang J. Advances of carbon materials as loaders for transition metal oxygen/sulfide anode materials. Chin J Rare Met. 2021;45(10):1241. https://doi.org/10.13373/j.cnki.cjrm.XY20040016.
[129] Tian X, Lu XF, Xia BY, Lou XW. Advanced electrocatalysts for the oxygen reduction reaction in energy conversion technologies. Joule. 2020;4(1):45. https://doi.org/10.1016/j.joule.2019.12.014.